The effect of spacing on the vortex-induced vibrations of two tandem flexible cylinders

Enhao Wang, , Qing Xiao, , Qiang Zhu, and , and Atilla Incecik

Citation: Physics of Fluids **29**, 077103 (2017); doi: 10.1063/1.4995463
View online: http://dx.doi.org/10.1063/1.4995463
View Table of Contents: http://aip.scitation.org/toc/phf/29/7
Published by the American Institute of Physics

The effect of spacing on the vortex-induced vibrations of two tandem flexible cylinders

Enhao Wang,[1] Qing Xiao,[1,a)] Qiang Zhu,[2] and Atilla Incecik[1]
[1]*Department of Naval Architecture, Ocean and Marine Engineering, University of Strathclyde, Glasgow, Scotland G4 0LZ, United Kingdom*
[2]*Department of Structural Engineering, University of California San Diego, La Jolla, California 92093-0085, USA*

(Received 12 February 2017; accepted 8 July 2017; published online 31 July 2017)

Vortex-induced vibrations (VIVs) of two flexible cylinders arranged in tandem are studied using a two-way fluid-structure interaction (FSI) method with different spacing ratios (S_x/D) at Reynolds number Re = 500 using a two-way fluid-structure interaction (FSI) method. The main objective of this study is to investigate the effect of spacing on the hydrodynamic interactions and the VIV responses of these cylinders. The responses of the two flexible cylinders are found to be similar to the classical VIV responses at small S_x/D. Once S_x/D is large enough for the vortices to become detached from the upstream cylinder, the response of the upstream cylinder is similar to the typical VIV response whereas the downstream cylinder undergoes wake-induced vibration. The characteristics of the response of the downstream cylinder in the present study are similar to those of the first two response regimes classified by previous researchers. The third regime is not observed for the flexible downstream cylinder with both ends fixed. The two changes in the phase relation between the cross-flow displacements of the two tandem flexible cylinders are discovered to be linked with the initial-upper branch transition and the upper-lower branch transition, respectively. The correlation lengths of the two flexible cylinders decrease significantly in the transition range between the upper and lower branches. Three modes of vortex shedding (2S, P + S, and 2P) have been identified in the present study. The upper-branch 2P mode is found to be associated with large-amplitude vibration of the upstream cylinder and the P + S mode is observed to be related to large-amplitude vibration of the downstream cylinder for S_x/D = 3.5 and 5. On the other hand, the lower-branch 2P mode leads to small-amplitude vibration of the downstream cylinder in the post-lock-in range at S_x/D = 2.5. The relative phase shifts of the sectional lift coefficients on different spanwise cross sections can be attributed to the variation of the vortex shedding flow along the flexible cylinders, and these phase shifts result in poor phasing between the forces and the displacements that is related to the decrease of the correlation lengths. *Published by AIP Publishing.* [http://dx.doi.org/10.1063/1.4995463]

I. INTRODUCTION

Vortex-induced vibration (VIV) of a single cylinder has been extensively studied by various researchers over the past few decades and comprehensive reviews can be found in Blevins,[1] Sarpkaya,[2] Bearman,[3] Williamson and Govardhan,[4] Gabbai and Benaroya,[5] Sumer and Fredsøe,[6] Bearman,[7] Wu *et al.*,[8] Païdoussis *et al.*,[9] and Triantafyllou *et al.*[10] However, there are many engineering problems that involve clusters of cylindrical structures being arranged in tandem configurations. The examples include heat exchanger tubes, chimney stacks, offshore structures, and transmission lines. Due to its practical significance, more and more studies are carried out on the VIV of multiple tandem cylinders.

Compared to a single cylinder, the flow past two tandem cylinders is much more complex due to the introduction of a new geometric parameter, i.e., the spacing between the cylinders (S_x). There are a number of flow regimes depending on the spacing between the two cylinders.[11,12] For two stationary cylinders in tandem arrangement, three major types of flow patterns have been identified. When the two cylinders are placed in very close proximity, the two cylinders behave as a single body. The separated shear layers from the upstream cylinder wrap around the downstream cylinder without reattaching onto its surface and form a single Kármán vortex street in the wake. With the increase in the spacing, the separated shear layers from the upstream cylinder reattach onto the surface of the downstream cylinder. When the spacing between the cylinders increases beyond a critical spacing, vortex shedding occurs in the gap region between the two cylinders so that the wake behind the cylinders is a combination of the wakes of the two cylinders.

Some experimental studies have been conducted to investigate the interference between two rigid circular cylinders undergoing VIV. Hover and Triantafyllou[13] and Assi *et al.*[14,15] considered the effect of the upstream cylinder wake on the response of the downstream cylinder. In their investigations, the upstream cylinder was stationary whilst the downstream cylinder was elastically mounted and free to vibrate in the

a)Author to whom correspondence should be addressed: qing.xiao@strath.ac.uk. Tel.: +44 01415484779.

cross-flow direction only. In Hover and Triantafyllou,[13] the downstream cylinder was placed at 4.75D behind the upstream cylinder and the Reynolds number was Re = 3×10^4. Large-amplitude galloping response was observed for the downstream cylinder. The results also indicated that the frequency lock-in began at a low reduced velocity (V_r), which was nearly the same as a single cylinder and its range extended to a V_r of at least 17. A phase change in the lift force, which was typically associated with the frequency lock-in, occurred at higher V_r. The force spectra suggested that the shedding from the upstream cylinder was not affected by motions of the downstream cylinder. Assi *et al.*[14] elaborated the excitation mechanism of wake-induced vibration (WIV) of the downstream cylinder. The Reynolds number in their study was up to 3×10^4. They suggested that the WIV of the downstream cylinder was excited by the unsteady vortex-structure interactions between the body and the upstream wake. In a recent research by Assi *et al.*,[15] the authors investigated how the cylinder responded to the vortex-structure interactions excitation. They introduced the concept of wake stiffness and concluded that it was the wake stiffness phenomenon that defined the character of the WIV response. Zdravkovich[16] studied the VIV of two elastically mounted rigid cylinders in tandem arrangement with different centre-to-centre spacing ratios (S_x/D) in the Re range of 10^4–10^5. It was observed that for a very small S_x/D up to 1.1, the two cylinders acted as a single body. With a slight increase in S_x/D up to 1.6, the shear layers from the upstream cylinder reattached onto the downstream cylinder. A bistable regime was found when S_x/D varied from 2.5 to 4, which indicated the minimum spacing required for the upstream cylinder to have regular vortex shedding. In this regime, the oscillation amplitudes of the upstream cylinder were larger than those of the downstream cylinder. For S_x/D larger than 4, the response of the upstream cylinder was smaller and less regular than that of the downstream cylinder.

The interference has also been considered for vibrating flexible cylinders. Brika and Laneville[17,18] investigated the VIV of a long flexible circular cylinder immersed in the wake of an identical stationary cylinder. S_x/D between the two cylinders ranged from 7 to 25 and Re ranged from 5000 to 27 000. It was found that the response of the flexible cylinder was no longer hysteretic and showed a single branch with a wider synchronization region that decreased with the increase in the spacing between the two cylinders. The onset of the synchronization shifted to higher V_r compared with the case of an isolated cylinder. Brika and Laneville[17] also considered the case in which both cylinders were allowed to vibrate. In that case, the response of the downstream cylinder became hysteretic. Huera-Huarte and Bearman[19] and Huera-Huarte and Gharib[20] experimentally studied the vortex- and wake-induced vibrations of two tandem flexible cylinders with near and far wake interferences in a Re range up to 12 000. It was found that the responses of both cylinders showed classical VIV resonance when V_r was close to the typical lock-in reduced velocities. When S_x/D is small, the maximum vibration amplitude of the upstream cylinder is higher than that of the downstream cylinder and the maximum vibration amplitude of the upstream cylinder increased with the decrease in spacing. For a large S_x/D, the response of the downstream cylinder exhibited non-classical VIV resonance with large amplitudes at high reduced velocities.

Apart from the experiments, there have also been a number of numerical studies on the VIV of two tandem cylinders. The majority of existing numerical studies were two-dimensional (2D) and focussed on one-degree-of-freedom (1DOF) cross-flow motions of rigid cylinders. Carmo *et al.*[21] conducted 2D numerical simulations of the flow around two tandem circular cylinders at Re = 150. The upstream cylinder was fixed and the downstream cylinder was free to vibrate in the transverse direction. S_x/D was varied from 1.5 to 8. Compared with an isolated cylinder, the downstream cylinder was found to have higher maximum amplitudes and wider lock-in ranges. The vibration amplitudes for higher V_r beyond the lock-in range were very significant. Carmo *et al.*[22] investigated the VIV of a cylinder that was completely free to move in the cross-flow direction (i.e., with no spring or damper attached to it) subject to the wake of an identical stationary cylinder. A fixed spacing ratio $S_x/D = 4$ was considered and Re varied from 100 to 645. Three different regimes were identified in their 2D simulations. A monotonically decreasing amplitude with increasing Re was observed in the first regime ($90 \le \mathrm{Re} \le 165$). The second regime was characterised by significant scatter in the vibration amplitude and its range is from Re ≈ 180 to Re = 360. Gradual transition between the second and third regimes took place for $360 \le \mathrm{Re} \le 405$. The third regime extended up to the highest Re tested. The amplitude was found to grow monotonically with Re. Zhao[23] presented the results of VIV of two rigidly coupled circular cylinders in tandem arrangement with four spacing ratios ranging from 1.5 to 6 at Re = 150. The results showed that the gap between the two cylinders had a significant effect on the response. When two rigidly coupled tandem cylinders were subject to VIV, the critical spacing for vortex shedding from the upstream cylinder was significantly smaller than that for two tandem stationary cylinders. The vortex shedding from the upstream cylinder took place at $S_x/D = 2$ in the lock-in range, and the lock-in range was found to be narrower than that of a single cylinder for $S_x/D = 1.4$ and 2 and wider for $S_x/D = 4$ and 6. Ding *et al.*[24] used 2D unsteady Reynolds-averaged Navier-Stokes (RANS) equations with the Spalart-Allmaras turbulence model to study the effect of tandem spacing on the VIV of two cylinders with passive turbulence control in the Re range of 30 000–100 000. The spacing between the cylinders varied from 2D to 6D. The numerical simulation successfully predicted all the ranges of responses including VIV and galloping. Furthermore, the results agreed well with the experimental measurements. The influence of the downstream cylinder on the amplitude and frequency responses of the upstream cylinder was found to be negligible when the spacing is larger than 2D. A rising trend of the vibration amplitude of the downstream cylinder was observed in all the cases when $2 \times 10^4 < \mathrm{Re} < 3 \times 10^5$. The galloping branch merged with the VIV upper-branch for spacing larger than 3D. Vortex structures showed significant variation in different flow regimes.

Two-degree-of-freedom (2DOF) VIV of two tandem rigid cylinders has also been studied using 2D numerical simulations. Papaioannou *et al.*[25] studied the effect of spacing on the

VIV of two rigid cylinders in tandem arrangement. The computations were carried out for S_x/D in the range of 2.5–5 at Re = 160. It was observed that the range of the response region of the upstream cylinder became wider with the decrease of S_x/D. The synchronization curve shifted on the V_r axis depending on the spacing. There was an increase in the maximum vibration amplitude of the downstream cylinder when the cylinders were brought to the spacing corresponding to the reattachment regime in the stationary system. Prasanth and Mittal[26] investigated the VIV of two circular cylinders in tandem arrangement with S_x/D = 5.5 at Re = 100 using a 2D stabilised finite element method (FEM). V_r ranged from 2 to 15. The downstream cylinder was found to undergo large-amplitude vibrations in both the in-line and cross-flow directions. Lock-in and hysteresis were observed for both the upstream and downstream cylinders. The large-amplitude vibrations of the downstream cylinder were maintained even beyond the lock-in range. The phase difference between the cross-flow displacement and the lift force went through an 180° jump in the middle of the synchronization regimes of both cylinders. The flow regime was divided into five sub-regimes based on the phase difference and the flow patterns. Bao *et al.*[27] studied the 2DOF VIV of two tandem cylinders with varying natural frequency ratios at Re = 150 by solving the 2D incompressible Navier-Stokes equations using a characteristic-based-split FEM. The spacing between the two cylinders was 5D. They found that the in-line response of the downstream cylinder was more sensitive to the natural frequency ratio than that in the transverse direction. As dual resonance was excited, the vortex shedding of the upstream cylinder in the tandem arrangement might show a P + S pattern, which strongly suppressed the vortex shedding of the downstream cylinder.

Compared with the popularity of 2D numerical studies, three-dimensional (3D) numerical simulations of VIV of two tandem cylinders have received less attention. Carmo *et al.*[21] compared the 3D numerical simulation results of VIV of a rigid cylinder exposed to an upstream stationary cylinder wake at Re = 300 with their 2D simulation results at Re = 150. For all the configurations investigated, they observed that the 3D results follow the same trend as the 2D results. However, the flow field was strongly three-dimensional for most of the configurations. Therefore, they concluded that 3D simulations were strictly necessary in order to obtain accurate values of forces or structural response. Carmo *et al.*[22] carried out 3D numerical simulations with the same parameters as their 2D calculations in the same study. The results showed that the variation of amplitude within the Re range tested was very small. The oscillation frequency of the downstream cylinder and the shedding frequency of the upstream cylinder were constant and had the same value throughout the entire Re range. The amplitudes observed in the 3D results are smaller than those observed in the 2D results for the same Re, which, according to the authors, was caused by the weakening of the spanwise vortices.

There are even fewer numerical studies on the VIV of two tandem flexible cylinders. Chen *et al.*[28] simulated VIV and WIV for two vertical risers in tandem and side-by-side arrangements at Re = 8400 using an unsteady RANS numerical method in conjunction with a chimera domain decomposition approach with overset grids. The in-line and cross-flow responses of the risers were calculated using a tensioned beam motion equation. For two vertical risers in tandem arrangement, the vortex street was suppressed between the risers and there was a reattachment of the shear layers to the downstream riser when S_x/D = 3. When S_x/D increased to 4, a vortex street started to appear in the gap between the risers with intermittent reattachment of shear layers on the downstream riser surface. In general, the computed vortex patterns and dynamic responses of the risers were in good agreement with the experimental data. González *et al.*[29] presented the results of their numerical simulation attempts for the experimental campaigns on a tandem arrangement of flexible cylinders by Huera-Huarte *et al.*[30] at Re = 16 000. The numerical simulation qualitatively reproduced the physical phenomena. However, the numerical model oversimplified the mechanical complexity of the flexible cylinder and the application of the axial tensions caused the numerical instability of the computation. Therefore, the authors suggested that future research was required in order to make a quantitative comparison with the experimental data.

Overall, VIV of two elastically mounted rigid cylinders in tandem arrangement has been widely studied both experimentally and numerically. Due to the complexity of the problem, there have been fewer studies on the VIV of two tandem flexible cylinders and most of the existing publications are experiments. Fully 3D fluid-structure interaction (FSI) simulations of VIV of two tandem flexible cylinders that can accurately predict the responses of the cylinders as well as provide the instantaneous 3D flow structures that are difficult to obtain in the experiments are still quite limited.

In this study, cross-flow VIV of two flexible cylinders in tandem arrangement at Re = 500 is investigated using a 3D numerical method. The choice of Re stems from the consideration that the flow around the cylinders is 3D, and it can be modelled by directly solving the 3D Navier-Stokes equations. We focussed on the V_r range of V_r = 4–10, in which the cylinders will mainly vibrate in the first mode. The main objective of the present work is to numerically study the effect of spacing on the hydrodynamic interactions and VIV responses of the two tandem flexible cylinders. Particular attention is paid to the aspects that have not been fully addressed by previous studies such as the correlation lengths and the time-dependent 3D flow structures.

II. NUMERICAL METHODS AND PROBLEM DESCRIPTION

The FSI simulation in the present study is carried out using the ANSYS MFX multi-field solver.[31] The governing equations for the flow around the flexible cylinders are the 3D unsteady incompressible Navier-Stokes equations. The Arbitrary Lagrangian-Eulerian (ALE) scheme is employed to deal with the moving boundaries of the flexible cylinders. The ALE form of the governing equations in the Cartesian coordinate system can be expressed as

$$\frac{\partial u_i}{\partial x_i} = 0, \tag{1}$$

$$\frac{\partial u_i}{\partial t} + \left(u_j - \hat{u}_j\right)\frac{\partial u_i}{\partial x_j} = -\frac{1}{\rho}\frac{\partial p}{\partial x_i} + \nu\frac{\partial^2 u_i}{\partial x_j^2}, \tag{2}$$

where x_i represents the Cartesian coordinate with $(x_1, x_2, x_3) = (x, y, z)$, u_i is the velocity component in the x_i-direction, $\hat{u}_i$ is the grid velocity component in the x_i-direction, p is the pressure, t is the time, ρ is the fluid density, and ν is the kinematic viscosity of the fluid.

The Navier-Stokes equations are discretised with an element-based finite volume method (FVM).[32] Rhie-Chow interpolation[33] is used to obtain pressure-velocity coupling on collocated grids. A second-order backward Euler scheme is adopted for the temporal discretisation and a high resolution scheme is used as the convection scheme that can be cast in the following form:

$$\varphi_{ip} = \varphi_{up} + \beta\nabla\varphi \cdot \Delta\mathbf{r}, \tag{3}$$

where φ_{up} is the value at the upwind node, $\nabla\varphi$ is the control volume gradients evaluated by Gauss' divergence theorem and $\Delta\mathbf{r}$ is the vector from the upwind node to the integration point ip. In the high resolution scheme, a nonlinear recipe for β based on the boundedness principles by Barth and Jespersen[34] is used.

Figure 1(a) shows the computational domain used in the computational fluid dynamics (CFD) simulation. The origin of the Cartesian coordinate system is located at the centre of the bottom end of the upstream cylinder as shown in Fig. 1(a). The

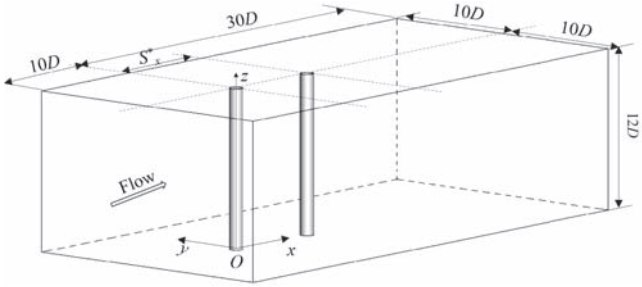

(a)

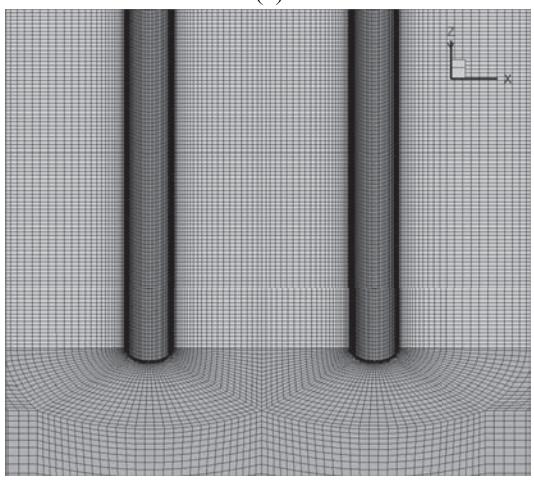

(b)

FIG. 1. (a) Computational domain and (b) computational mesh in the CFD simulation.

length of the computational domain is $40D$ in the streamwise direction (x-direction) with the upstream cylinder located at $10D$ downstream the inlet boundary. The width of the domain in the cross-flow direction (y-direction) is 20D and the computational domain size in the spanwise direction (z-direction) is set to the cylinder length, which is $12D$. The computational mesh for $S_x/D = 5$ used in the CFD simulation is shown in Fig. 1(b). The boundary conditions for the governing equations are as follows. The surfaces of the cylinders are assumed to be smooth, where no-slip boundary conditions are employed. Apart from the no-slip boundary conditions, the cylinder surfaces are also set to be fluid-solid interfaces where force and displacement data are transferred. The inlet velocity boundary condition is set to be the same as the freestream velocity. At the outflow boundary, the gradients of the fluid velocity in the streamwise direction are set to zero. On the two transverse boundaries, the velocity in the direction normal to the boundary is zero and a periodic boundary condition is imposed on the top and bottom boundaries. As for the pressure boundary conditions, the normal gradient of pressure is zero on the cylinder surfaces, the inlet boundary, and the transverse boundaries. The pressure at the outflow boundary is given a reference value of zero.

In the present study, the two flexible cylinders are modelled as beams fixed at the two ends and they are free to vibrate in the transverse direction. The vibrations of the cylinders satisfy the Euler-Bernoulli beam theory. The transverse motions of the two flexible cylinders can be described as

$$\frac{\partial^2}{\partial z^2}\left[EI\frac{\partial^2 y}{\partial z^2}\right] + m\frac{\partial^2 y}{\partial t^2} + c\frac{\partial y}{\partial t} = F_y, \tag{4}$$

where E is Young's modulus, I is the moment of inertia, m is the mass per unit length, c is the structural damping, z is the undeflected cylinder axial coordinate, y is the transverse displacement, and F_y is the hydrodynamic force in the transverse direction. The boundary conditions for Eq. (4) in the case of a beam fixed at the two ends are

$$\begin{aligned} &y(0,t) = 0,\ y(L,t) = 0 \qquad \forall t, \\ &\frac{\partial y(0,t)}{\partial z} = 0,\ \frac{\partial y(L,t)}{\partial z} = 0 \quad \forall t. \end{aligned} \tag{5}$$

A finite element method is used to discretise the finite element analysis (FEA) models and the corresponding global equation system is given by

$$\mathbf{M}\ddot{\mathbf{q}} + \mathbf{C}\dot{\mathbf{q}} + \mathbf{K}\mathbf{q} = \mathbf{F}, \tag{6}$$

where $\mathbf{q}$ is the nodal displacement vector and a dot denotes differentiation with respect to time. The global mass, damping, and stiffness matrices ($\mathbf{M}$, $\mathbf{C}$, and $\mathbf{K}$) are the collective effects of the individual elements' mass, damping, and stiffness matrices ($\mathbf{M}^e = \iiint \mathbf{N}^T \rho_s \mathbf{N} \mathrm{d}x\mathrm{d}y\mathrm{d}z$, $\mathbf{C}^e = \iiint \mathbf{N}^T c \mathbf{N} \mathrm{d}x\mathrm{d}y\mathrm{d}z$, and $\mathbf{K}^e = \iiint \mathbf{B}^T \mathbf{E} \mathbf{B} \mathrm{d}x\mathrm{d}y\mathrm{d}z$, where $\mathbf{N}$ is the matrix of shape functions, ρ_s is the structural density, $\mathbf{B}$ is the strain-displacement matrix, and $\mathbf{E}$ is the elasticity matrix) derived from the principle of virtual work. $\mathbf{F}$ is the hydrodynamic force vector. The governing equation is solved using the Hilber-Hughes-Taylor (HHT) method[35] with a second-order accuracy.

A 3D 20-node solid element that exhibits quadratic displacement behaviour is used for the discretisation of the FEA

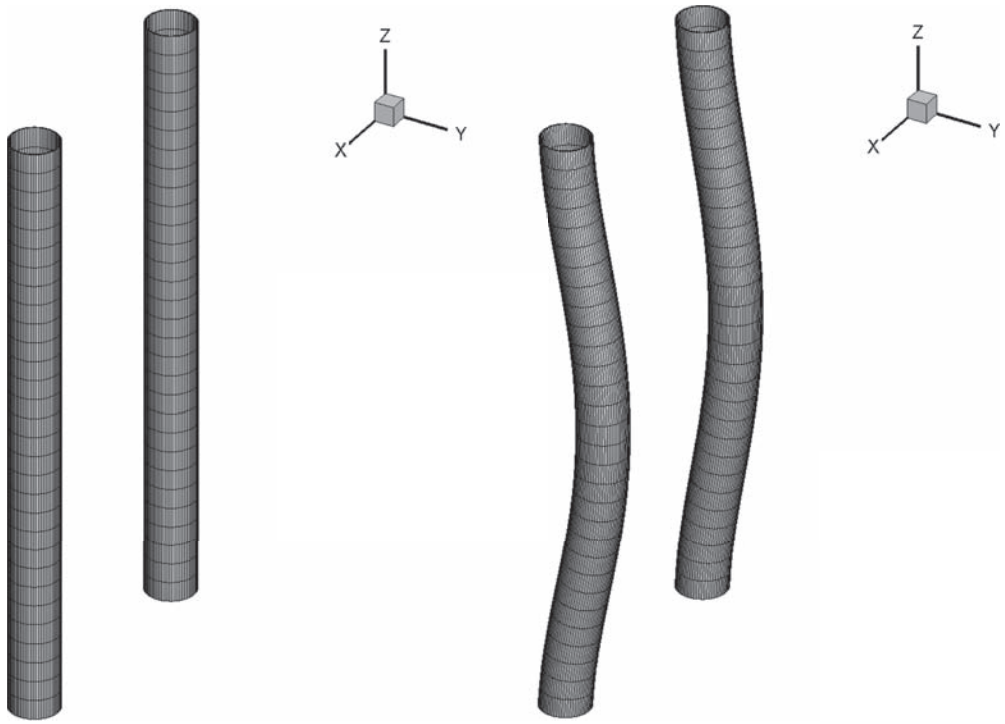

FIG. 2. Computational mesh in the FEA simulation at $S_x/D = 5$: (a) initial configuration and (b) mesh after deflections.

models of the flexible cylinders. The element is defined by 20 nodes having three degrees of freedom per node: translations in the nodal x-, y-, and z-directions.[36] Figures 2(a) and 2(b) show the finite elements of the two tandem flexible cylinders for $S_x/D = 5$ in the initial configuration and after deflections, respectively. In the solid domain, the surfaces of the cylinders are also set to be fluid-solid interfaces for data transfer.

To accommodate the motions of the flexible cylinders, the displacement diffusion model[37–39] for mesh motion is adopted. The displacements of the mesh points are calculated based on the following equation:

$$\nabla \cdot \left(\Gamma \nabla S_y\right) = 0, \tag{7}$$

where S_y represents the displacements of the nodal points in the cross-flow direction, Γ is the mesh stiffness. In this study, in order to avoid excessive deformation of the near-wall elements, the parameter Γ is set to be $\Gamma = 1/\forall^2$ where $\forall$ is the control volume size.

A two-way explicit approach is utilized for the FSI simulation in the present study. Detailed solution procedures of this approach can be described as follows. At the beginning of each time step, the flow equations are solved to obtain the forces on the flexible cylinders. Then the forces are interpolated to the FEA mesh using the conservative interpolation, and the global equation system for structural dynamics is solved to obtain the quantities of cylinder motions. After that the displacements are interpolated to the CFD mesh with the profile preserving interpolation, and the positions of the mesh points are calculated and updated using Eq. (7). The next time step begins with solving the flow equations on the updated mesh. Such an FSI loop is repeated until the last time step of the simulation.

VIV of two tandem flexible cylinders is investigated numerically. Two identical flexible cylinders with diameter D and length L are aligned in the direction of the flow in their rest positions. To simplify the problem, the vibrations of the cylinders are confined to the cross-flow direction. Similar simplifications have been adopted by previous researchers such as Evangelinos and Karniadakis,[40] Evangelinos *et al.*,[41] and Xie *et al.*[42] to study the VIV of a flexible cylinder. The length-to-diameter ratio is $L/D = 12$, which allows the discretisation of the cylinder span with a fine mesh to resolve the characteristics of the flow with acceptable computational efforts. Moreover, $L/D = 12$ is also comparable to L/D values used by Evangelinos *et al.*[41] and Xie *et al.*[42] in their numerical studies. A moderate mass ratio $m^* = 4m/\rho\pi D^2 = 10$ is considered. The influence of the structural damping is mainly reflected in the maximum vibration amplitude and in order to maximize the vortex-induced responses of the flexible cylinders, the structural damping is set to zero. The Reynolds number is defined as $\mathrm{Re} = VD/\nu$ where V is the freestream velocity and a constant Reynolds number $\mathrm{Re} = 500$ is adopted in the present simulation. The reduced velocity $V_r = V/f_1 D$ ranges from 4 to 10. Here, f_1 is the fundamental natural frequency (i.e., the first eigenfrequency) of the flexible cylinder and for a beam with two fixed ends, $f_1 = \frac{1}{2\pi}\left(1 + \frac{\pi}{2}\right)^2 \sqrt{\frac{EI}{mL^4}}$. Since V is fixed in the present study, the bending stiffness EI is varied in each simulation to obtain the corresponding f_1 of the desired

V_r. In order to study the effect of spacing on the VIV of two tandem flexible cylinders, three different centre-to-centre spacing ratios are selected, i.e., S_x/D = 2.5, 3.5, and 5 as in Papaioannou *et al.*[25] These three spacing ratios are based on different regimes in the stationary system. S_x/D = 2.5 belongs to the reattachment regime where the shear layers from the upstream cylinder reattach onto the surface of the downstream cylinder; S_x/D = 5 represents the binary-vortex regime where the separated shear layers of the upstream cylinder roll up in the gap region and a binary vortex street is formed behind the downstream cylinder consisting of the interacting wakes of the two cylinders and the spacing S_x/D = 3.5 is very close to the critical spacing of transition from the reattachment regime to the binary-vortex regime.

To confirm the flow regimes for the three spacing ratios predicted by the present methods, flow past two tandem stationary cylinders at Re = 500 was simulated and the spanwise mean drag coefficients (C_{Dmean}) were compared with the numerical results of Papaioannou *et al.*[43] in Fig. 3. It can be seen that the present results are in good agreement with those of Papaioannou *et al.*[43] In the reattachment regime, C_{Dmean} of the upstream cylinder decreases with the increase in the spacing and the value of C_{Dmean} experiences a jump at the critical spacing. This jump is more pronounced on C_{Dmean} of the downstream cylinder, which changes from negative to positive. Figures 4 and 5 show the 3D flow structures and the vortex shedding at z/L = 0.5 around stationary cylinders. The present results agree with the descriptions of the different flow patterns for two tandem stationary cylinders by Igarashi,[12] Igarashi,[44] Zdravkovich,[11] Papaioannou,[45] Xu and Zhou,[46] Zhou and Yiu,[47] Carmo *et al.*,[48] Carmo *et al.*,[49] and Sumner.[50]

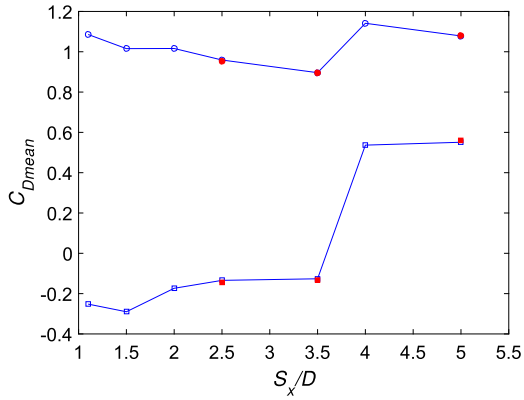

FIG. 3. Comparison of spanwise mean drag coefficients of two tandem stationary cylinders at Re = 500: blue open circles—upstream cylinder (Papaioannou *et al.*); blue open squares—downstream cylinder (Papaioannou *et al.*); red filled circles—upstream cylinder (present simulation); red filled squares—downstream cylinder (present simulation).

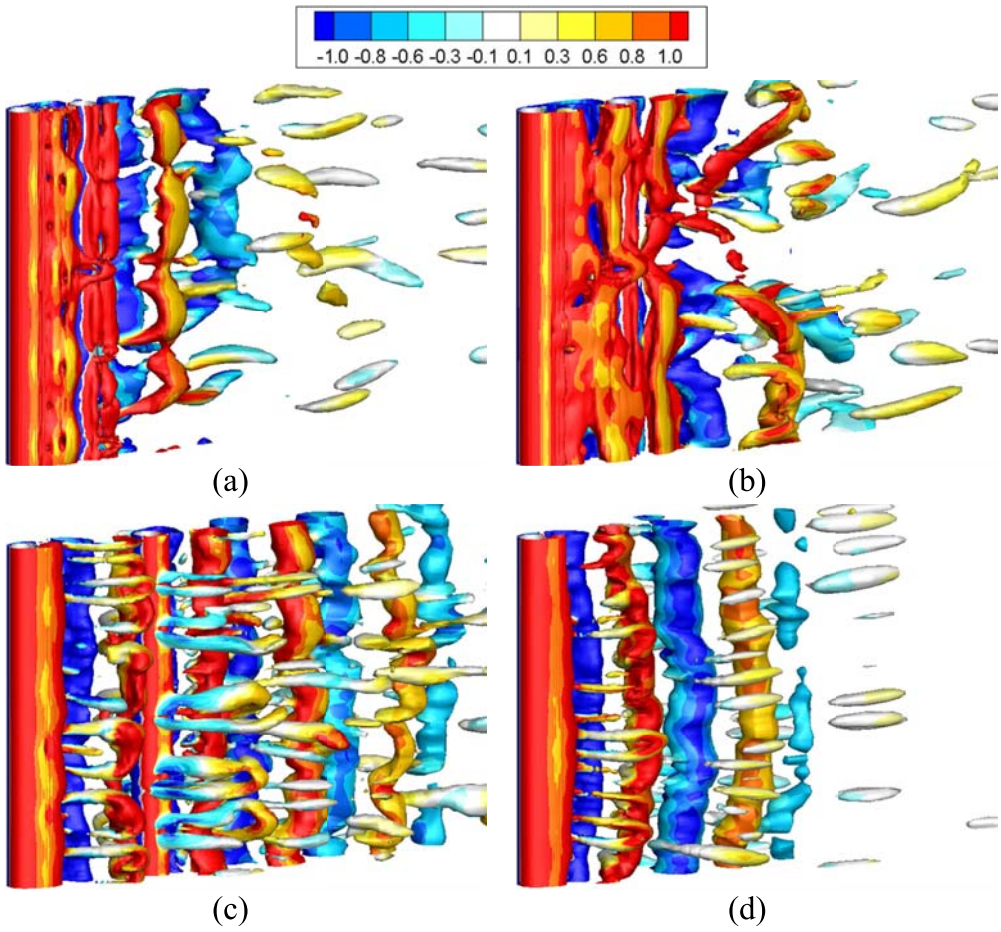

FIG. 4. Iso-surfaces of the eigenvalue $\lambda_2 = -0.1$ with the contours of the spanwise vorticity ω_z on the iso-surfaces for stationary cylinders: (a) S_x/D = 2.5, (b) S_x/D = 3.5, (c) S_x/D = 5, and (d) single cylinder.

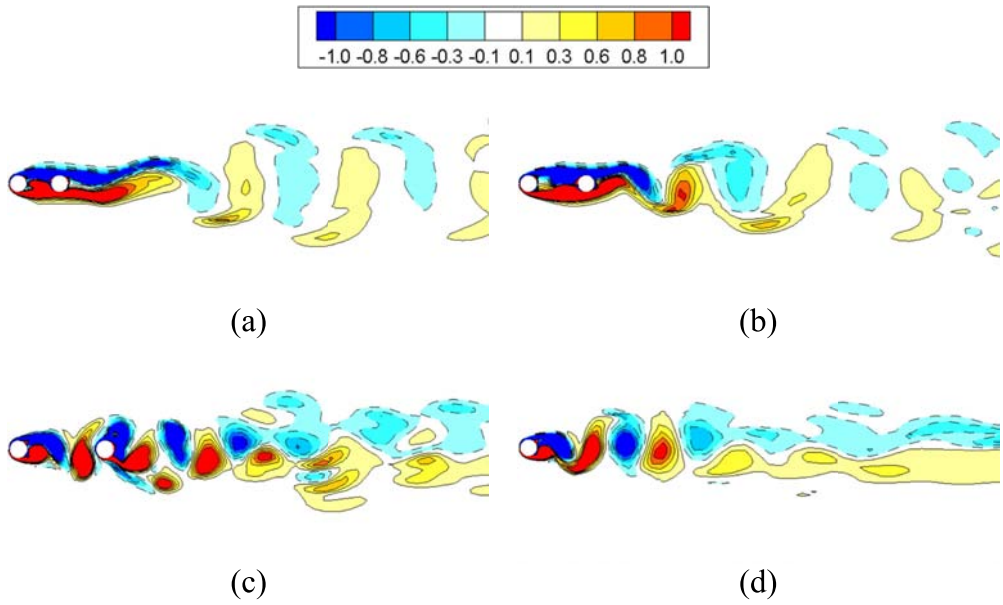

FIG. 5. Spanwise vorticity contours ω_z for stationary cylinders at $z/L = 0.5$: (a) $S_x/D = 2.5$, (b) $S_x/D = 3.5$, (c) $S_x/D = 5$, and (d) single cylinder.

III. VALIDATION AND MESH DEPENDENCY STUDY

The FSI solver has been used in our previous study[38] to investigate the VIV of a vertical riser with $L/D = 481.5$ in uniform and linearly sheared currents and the numerical results were compared with the ExxonMobil vertical riser model test results obtained at the MARINTEK by Lehn.[51] The numerical results were in good agreement with the experimental data. In the present study, further investigations on the cross-flow VIV of a single flexible cylinder with $m^* = 10$, $L/D = 12$, and two fixed ends at Re = 1000 were conducted using the present numerical methods and the results are compared with the numerical results by Xie *et al.*[42] in Fig. 6. It demonstrates that the present numerical methods are capable of accurately predicting VIV responses of flexible cylinders at early subcritical Reynolds numbers.

According to a series of publications on 3D numerical simulations of VIV of an elastically mounted circular cylinder,[37,52,53] the important mesh parameters in the CFD simulation are the number of nodes along the circumference of the cylinder N_c, the minimum mesh size next to the cylinder surface in the radial direction Δr, and the mesh size in the spanwise direction of the cylinder Δz. Similarly, the important mesh parameter in the FEA of the present FSI simulations is the number of segments along the cylinder span N_z. In order to evaluate the dependency of the numerical results on the CFD mesh parameters, simulations were carried out for the VIV of a single flexible cylinder with $m^* = 10$ and $L/D = 12$ at $V_r = 6$ and Re = 500 with three different CFD mesh systems while using the same FEA mesh with $N_z = 30$. The results computed using the different CFD meshes are tabulated in Table I. As shown in the table, the maximum difference of 3.36% occurs in the value of the spanwise root mean square (rms) lift coefficient C_{Lrms} between CFDM1 and CFDM2, whereas the maximum difference between CFDM2 and CFDM3 reduces to 1.4%. It can be concluded that the combination of $N_c = 120$, $\Delta r = 0.001D$, and $\Delta z = 0.1D$ is sufficient for the CFD simulation of VIV of flexible cylinders in the present study. Then, CFDM2 was used to study the dependency of the numerical results on the FEA mesh parameter. Three FEA meshes are generated with $N_z = 15$, 30, and 60. The comparison of the results computed with different FEA mesh parameters is shown in Table II. The maximum difference between FEAM1 and FEAM2 is observed in the spanwise rms drag coefficient C_{Drms} and takes the value of 1.14%. In contrast, the maximum difference between FEAM2 and FEAM3 is 0.55%, which appears in C_{Lrms}. Based on the FEA mesh dependency test results, $N_z = 30$ is used in the present study.

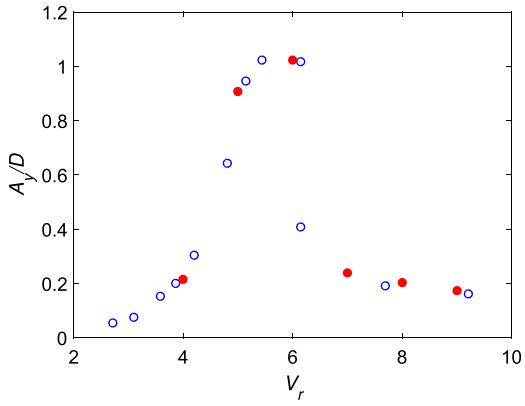

FIG. 6. Comparison of vibration amplitudes of a single flexible cylinder with $m^* = 10$, $L/D = 12$ at Re = 1000: blue circles—Xie *et al.*; red filled circles—present simulation.

TABLE I. CFD mesh dependency test results.

CFDM	N_c	$\Delta r/D$	$\Delta z/D$	A_y/D	C_{Dmean}	C_{Drms}	C_{Lrms}
1	80	0.002	0.2	0.7443	1.5975	0.2501	0.1717
2	120	0.001	0.1	0.7480	1.6127	0.2449	0.1661
3	160	0.0005	0.05	0.7524	1.6039	0.2482	0.1638

TABLE II. FEA mesh dependency test results.

FEAM	N_z	A_y/D	C_{Dmean}	C_{Drms}	C_{Lrms}
1	15	0.7515	1.5964	0.2421	0.1673
2	30	0.7480	1.6127	0.2449	0.1661
3	60	0.7480	1.6076	0.2453	0.1652

IV. RESULTS AND DISCUSSIONS

Numerical simulation was performed for the VIV of two flexible cylinders in tandem arrangement with three different spacing ratios (S_x/D = 2.5, 3.5, and 5) at an early subcritical Reynolds number Re = 500 for a reduced velocity range V_r = 4–10. The results are compared with those of a single flexible cylinder to investigate the effect of spacing on the hydrodynamic interactions and the VIV responses of the two tandem flexible cylinders.

A. Dominant modes

In order to investigate the dominant modes of the flexible cylinders and the contributions of each vibration mode to the overall dynamic responses, the modal amplitudes are computed using the same modal decomposition method as in Huera-Huarte and Bearman.[19,54] The modal analysis is based on the fact that the riser response can be expressed in the matrix form as a linear combination of its modes,

$$\mathbf{y}(z,t) = \mathbf{\Phi}(z)\,\mathbf{y}_M(t), \tag{8}$$

where $\mathbf{\Phi} = [\phi_1, \phi_2, \ldots, \phi_n]$ is the displacement modal-shape matrix, which is built by stacking the nondimensional mode shapes that are normalized to be 1 at its maximum as columns. $\mathbf{y}(z, t) = [y_1(z_1, t), y_2(z_2, t), \ldots, y_n(z_n, t)]$ is the measured displacement matrix whose row vectors are the time series of the measured displacements along the cylinder. $\mathbf{y}_M(t)$ is the modal contribution matrix containing the time series of each mode's contribution to the overall response as the row vectors $\mathbf{y}_M(t) = [y_{M1}(t), y_{M2}(t), \ldots, y_{Mn}(t)]$. We have

$$\mathbf{y}_M(t) = \mathbf{\Phi}^{-1}(z)\,\mathbf{y}(z,t). \tag{9}$$

Figure 7 illustrates the variation of the modal amplitudes of the first three modes with V_r. It can be observed from the figure that the dominant mode in most cases is the first mode. The contribution of the second mode is relatively small compared with that of the first mode at low V_r, but this increases gradually with the increase in V_r. At V_r = 10, the modal amplitude of the second mode overtakes that of the first mode for a single flexible cylinder. The contribution of the third mode remains small throughout the V_r range considered. Figure 8 shows the instantaneous nondimensional deflections of the flexible cylinders at V_r = 6. As shown in Fig. 8, all the vibrations at V_r = 6 demonstrate easily identifiable first mode characteristics. The instantaneous nondimensional deflections of the flexible cylinders at V_r = 10 are presented in Fig. 9. The vibration of a single flexible cylinder can be seen to be dominated by the second mode. Meanwhile, the vibrations of the two tandem flexible cylinders at V_r = 10 are not as regular as those at V_r = 6. The irregularity in the vibrations of the two flexible cylinders is due to the fact that contributions of the first and the second modes are comparable at V_r = 10.

B. Response amplitudes

In Huera-Huarte and Bearman,[19] the envelopes of the displacements are calculated using the analytical signals described by Pikovsky *et al.*[55] based on the use of Hilbert transforms, and the mean values of the envelopes are used to represent the vibration amplitudes (A_y/D). The same technique is adopted in the present study to determine the vibration amplitudes of the flexible cylinders. Figure 10 shows the time histories of the nondimensional displacements (y/D) on the different cross sections along the two tandem flexible cylinders when S_x/D = 5 and V_r = 6. The solid red lines are the envelopes of the signals and the dashed red lines represent the mean values of the envelopes inside the selected time window by which the sectional vibration amplitudes [$A_y(z)/D$] are denoted. A_y/D is determined by the maximum value of $A_y(z)/D$ along each cylinder. Figure 11 shows the variation of A_y/D with V_r for the two flexible cylinders arranged in tandem at different S_x/D. The results for a single flexible cylinder are also included for comparison. As the dominant mode in most of the cases considered in the present study is the first mode, the majority of A_y/D is observed at z/L = 0.5. The exceptions appear at V_r = 10 when the contribution of the second mode is of a similar order of magnitude to that of the first mode. As shown in Fig. 9, for two flexible cylinders in tandem arrangement, A_y/D appears around z/L = 0.4 and it shifts to $z/L \approx 0.3$ in the case of a single flexible cylinder where the second mode vibration dominates. In general, the A_y/D response curves in Fig. 11 are similar to the modal amplitude response curves of the first mode in Fig. 7 due to the fact that the first mode is the dominant mode in most cases.

The maximum vibration amplitudes (A_{ym}/D) of the upstream cylinder for S_x/D = 3.5 and 5 are observed at an identical reduced velocity V_r = 6 with a magnitude of $A_{ym}/D \approx 0.76$, which is similar to A_{ym}/D of a single flexible cylinder. As the spacing decreases to S_x/D = 2.5, A_{ym}/D of the upstream cylinder increases to 0.87. This increase in A_{ym}/D of the upstream cylinder with the decrease of S_x/D was also observed by Huera-Huarte and Bearman[19] in their experimental study with Re up to 12 000 and by Papaioannou *et al.*[25] in their 2D numerical simulation at Re = 160. Compared with the upstream cylinder, the effect of the hydrodynamic interactions between the two tandem flexible cylinders on the vibration amplitude responses of the downstream cylinder is more obvious. The maximum vibration amplitudes of the downstream cylinder for S_x/D = 3.5 and 5 are found to be similar ($A_{ym}/D \approx 1$). This is different from the results of Papaioannou *et al.*[25] in which the maximum vibration amplitude of the downstream cylinder in the case S_x/D = 3.5 is similar to that at S_x/D = 2.5. It is believed that this difference can be attributed to the difference in Re. Papaioannou *et al.*[25] considered a relatively low Reynolds number Re = 160. In contrast, the Reynolds number in the present simulation is Re = 500. According to Sumner,[50] the critical spacing $(S_x/D)_{cr}$ is particularly sensitive to the Reynolds number. Ljungkrona and Sundén[56] reported that $(S_x/D)_{cr}$ at Re = 160 is approximately 4.54 and decreases to $(S_x/D)_{cr} \approx 3.7$ when Re increases to 500. Therefore, S_x/D = 3.5 is further below the critical spacing ratio

in the study of Papaioannou *et al.*[25] than in the present study resulting in A_{ym}/D at $S_x/D = 3.5$ in their study being similar to that at $S_x/D = 2.5$.

In the present study, when S_x/D falls to 2.5, A_{ym}/D of the downstream cylinder increases to 1.1 and it shifts to a higher reduced velocity $V_r = 7$ due to the shielding effect of the upstream cylinder. When $V_r = 8$–10, for the three spacing ratios considered, the upstream cylinder shows a typical VIV response with very small vibration amplitudes at high V_r. In terms of the downstream cylinder, a lower-branch VIV response is observed for $S_x/D = 2.5$ and 3.5 due to the fact that the vortices impinging on the downstream cylinder are connected to the shear layers of the upstream cylinder as illustrated by the spanwise vorticity ($\omega_z = \partial u_2/\partial x_1 - \partial u_1/\partial x_2$) contours in Figs. 23(a) and 23(b). In contrast, at $S_x/D = 5$, the completely detached vortices from the upstream cylinder in Fig. 23(c) cause the WIV of the downstream cylinder with large-amplitude vibration being maintained until the maximum V_r considered in the present study. Assi *et al.*[15] classified the response of an elastically mounted downstream cylinder into three regimes: (i) before the vortex shedding frequency f_v = the natural frequency of the cylinder f_n, when the Strouhal number St = 0.2 is approaching f_n, the A_y/D response resembles the typical VIV response; (ii) the second regime, between $f_v = f_n$ and the equivalent natural frequency of the wake stiffness $f_w = f_n$, is marked by a steep slope in the A_y/D response curve; and (iii) the third regime beyond $f_w = f_n$ is characterised by a change of the slope in the response curve of A_y/D. According to their descriptions, the A_y/D response of the flexible downstream cylinder at $S_x/D = 5$ in Fig. 11 is similar to the first two regimes and the third regime is not observed in the present study and the possible reasons will be provided in Sec. IV C. We also notice that the present A_y/D in the second regime shows a plateau instead of increasing monotonically with V_r as shown in the experimental results of Hover and Triantafyllou[13] and Assi *et al.*[14,15] This discrepancy can be attributed to the different treatments of Re between the present study and the experiments. In the present

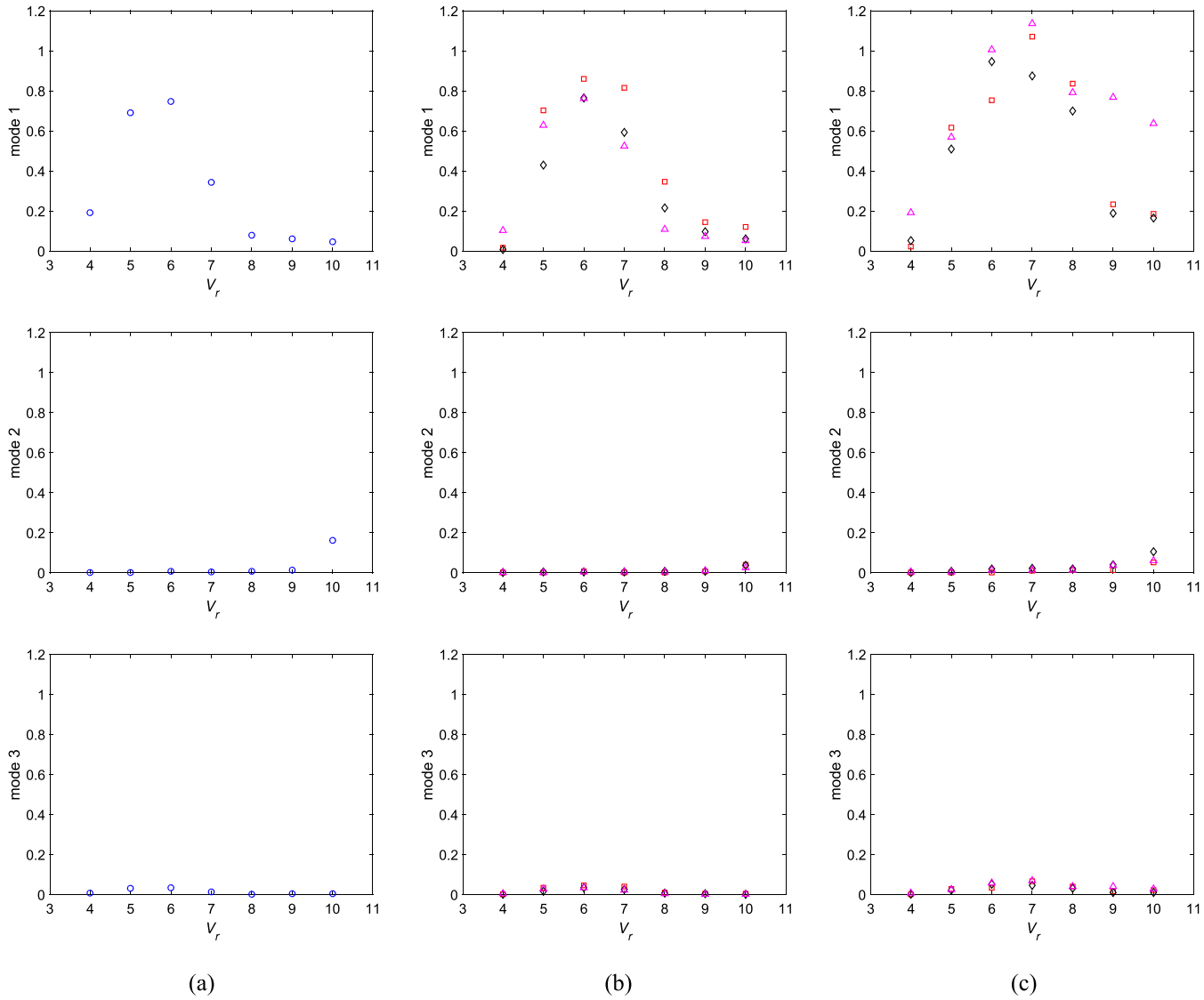

FIG. 7. Variation of modal amplitudes with V_r: (a) single flexible cylinder, (b) upstream cylinder, and (c) downstream cylinder. Blue circles—single flexible cylinder; red squares—tandem, $S_x/D = 2.5$; black diamonds—tandem, $S_x/D = 3.5$; pink triangles—tandem, $S_x/D = 5$.

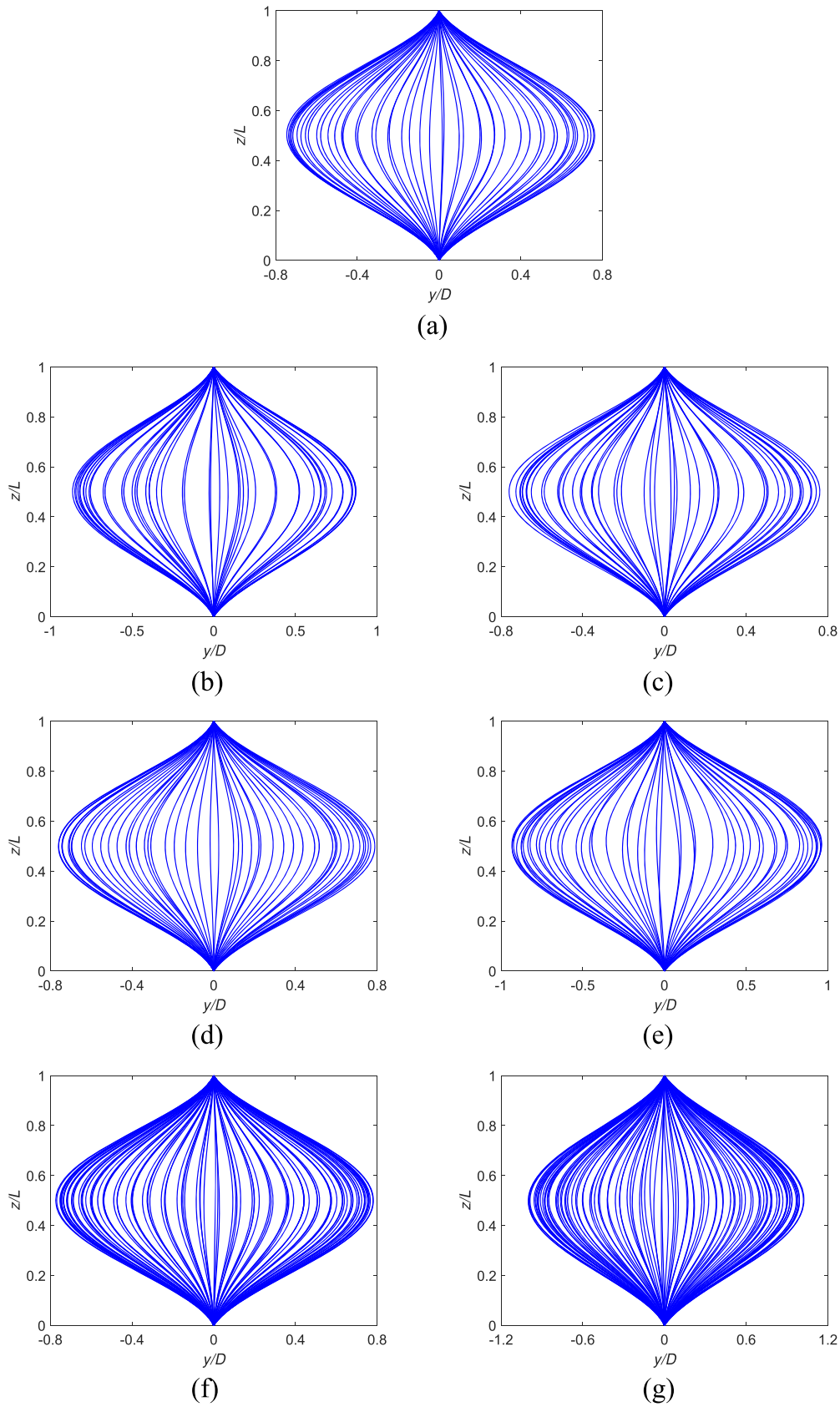

FIG. 8. Instantaneous nondimensional deflections of the flexible cylinders at $V_r = 6$: (a) single flexible cylinder, (b) upstream cylinder, $S_x/D = 2.5$, (c) downstream cylinder, $S_x/D = 2.5$, (d) upstream cylinder, $S_x/D = 3.5$, (e) downstream cylinder, $S_x/D = 3.5$, (f) upstream cylinder, $S_x/D = 5$, and (g) downstream cylinder, $S_x/D = 5$.

study, V and Re are fixed and EI is varied to obtain the desired V_r. In contrast, V, as well as Re, is usually increased in the experiment in order to increase V_r. Assi *et al.*[15] concluded that the increasing trend of the vibration amplitude in WIV is

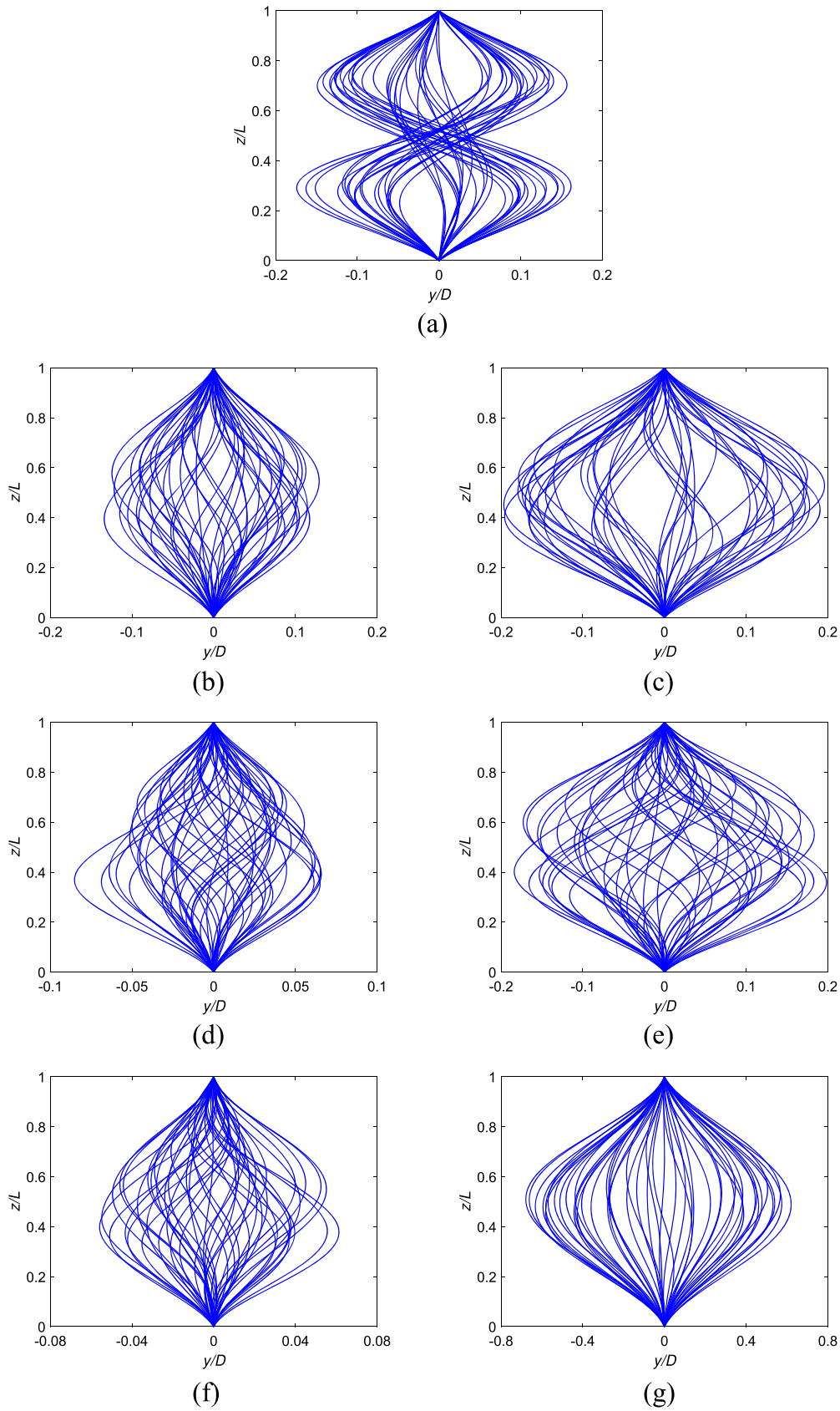

FIG. 9. Instantaneous nondimensional deflections of the flexible cylinders at V_r = 10: (a) single flexible cylinder, (b) upstream cylinder, S_x/D = 2.5, (c) downstream cylinder, S_x/D = 2.5, (d) upstream cylinder, S_x/D = 3.5, (e) downstream cylinder, S_x/D = 3.5, (f) upstream cylinder, S_x/D = 5 and (g) downstream cylinder, S_x/D = 5.

a direct effect of Re rather than V_r. Therefore, it is not surprising that the aforementioned difference in the A_y/D responses in the second regime exists between the present results and the experimental data.

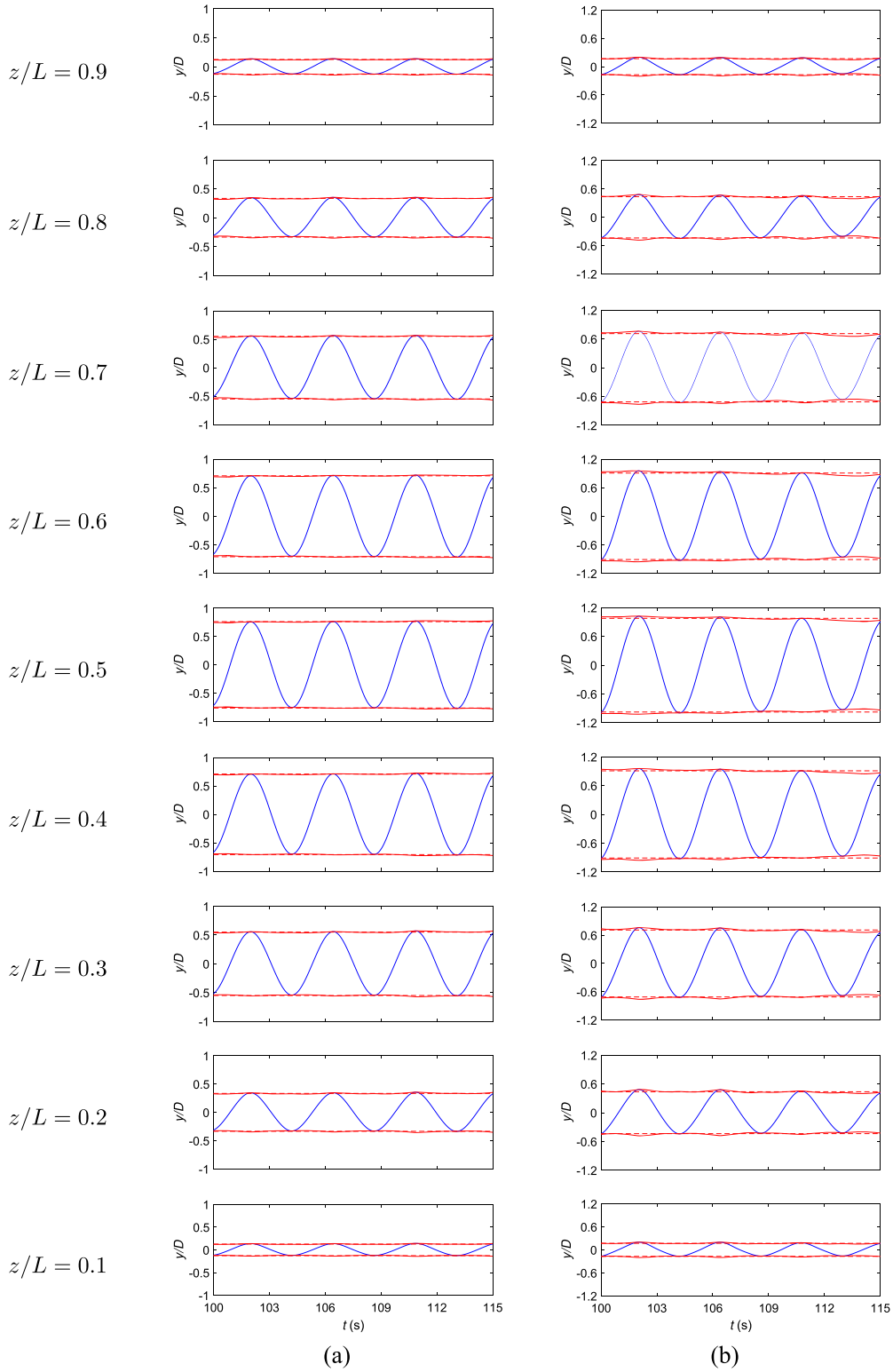

FIG. 10. Displacement time histories on different cross-sections along two tandem flexible cylinders at V_r = 6 and S_x/D = 5: (a) upstream cylinder and (b) downstream cylinder. Blue solid line— displacement signals; red solid line—envelopes of the signals; red dashed line—mean values of the envelopes.

C. Response frequencies

Spectral analysis is conducted for the time histories of the displacements after the eliminations of the transient responses. The oscillation frequencies (f_{oy}) are determined by the frequencies associated with the prominent peaks of the y/D amplitude spectra and then normalized using f_1. Figure 12 shows the comparison of the nondimensional oscillation frequencies (f_{oy}/f_1) between the two flexible cylinders in tandem arrangement and a single flexible cylinder. Based on the synchronization between f_{oy} and f_1, the lock-in range of the single flexible cylinder in terms of V_r is from 4 to 7. Within the lock-in range, f_{oy} locks into f_1 of the flexible cylinder. As V_r increases beyond the lock-in range, f_{oy} follows the Strouhal line. It can be

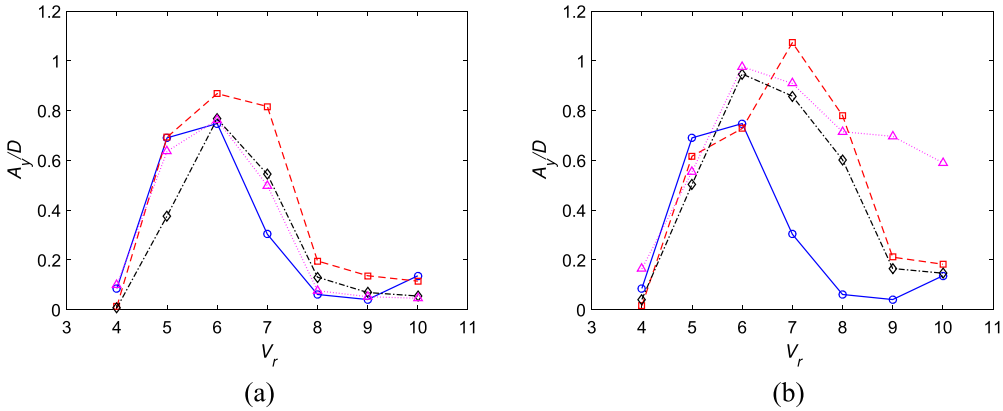

FIG. 11. Variation of the vibration amplitudes with V_r for flexible cylinders: (a) upstream cylinder and (b) downstream cylinder. Blue circles—single flexible cylinder; red squares—tandem $S_x/D = 2.5$; black diamonds—tandem, $S_x/D = 3.5$; pink triangles—tandem, $S_x/D = 5$.

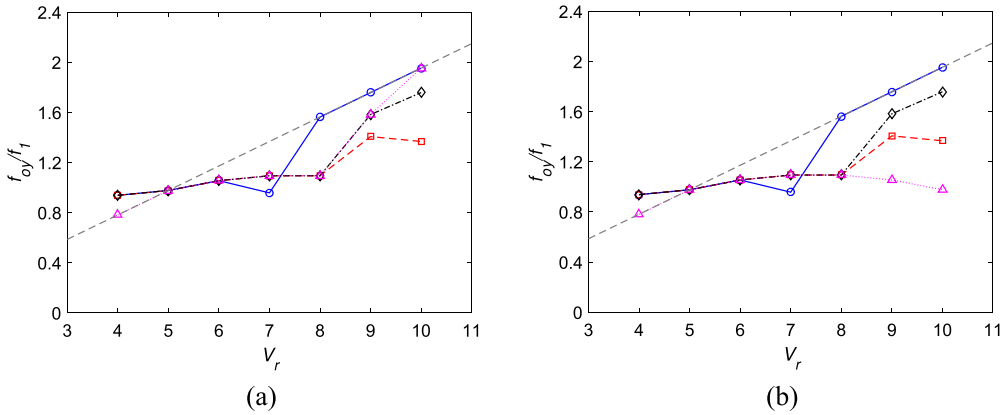

FIG. 12. Variation of oscillation frequencies with V_r for flexible cylinders: (a) upstream cylinder and (b) downstream cylinder. Grey dashed line—St = 0.2; blue circles—single flexible cylinder; red squares—tandem $S_x/D = 2.5$; black diamonds—tandem, $S_x/D = 3.5$; pink triangles—tandem, $S_x/D = 5$.

observed that the frequency response of a single flexible cylinder is similar to that of an elastically mounted circular cylinder reported by Zhao *et al.*[37] and Govardhan and Williamson.[57] For two tandem flexible cylinders, the lock-in ranges for $S_x/D = 2.5$ and 3.5 are identical (i.e., $V_r = 4$–8). When S_x/D increases to 5, the lock-in range of the upstream cylinder changes to $V_r = 5$–8. The synchronization of the downstream cylinder also starts at $V_r = 5$. However, it extends to the maximum V_r considered in the present simulation. The f_{oy}/f_1 response of the flexible downstream cylinder at $S_x/D = 5$ in Fig. 12 is also similar to the first two regimes described by Assi *et al.*:[15] in the first regime, f_{oy} follows the Strouhal line and in the second regime, f_{oy} remains rather close to f_1. As mentioned in Sec. IV B, the third regime characterised by $f_{oy} = f_w$ is not observed for the flexible downstream cylinder with two fixed ends in the present simulation. The reasons are as follows: unlike an elastically mounted rigid cylinder, a flexible cylinder has an infinite number of natural frequencies. In order for the third regime to occur, f_w needs to dominate all of the natural frequencies of a flexible cylinder, which is unrealistic. In addition, for a flexible downstream cylinder with two fixed ends, the natural frequencies of two neighbouring vibration modes are so close that when f_w surpasses the natural frequency of one mode, it is already within the bandwidth of the next mode. Therefore, it is expected that, with the increase in V_r, the response of the present flexible downstream cylinder will repeat the first two regimes for the different vibration modes.

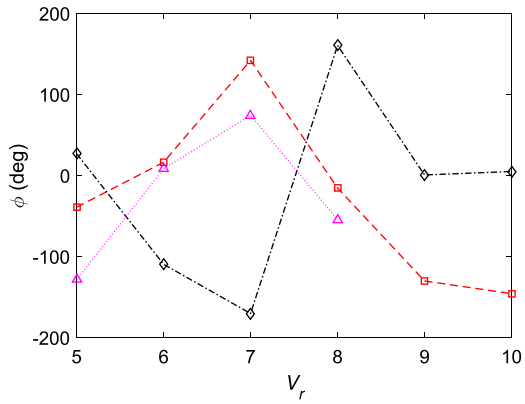

FIG. 13. Variation of phase differences ϕ between the cross-flow displacements at $z/L = 0.5$ of the two tandem flexible cylinders in the time range of $t = 100 - 115$ s with V_r: red squares—tandem $S_x/D = 2.5$; black diamonds—tandem, $S_x/D = 3.5$; pink triangles—tandem, $S_x/D = 5$.

Unlike the single flexible cylinder, f_{oy} of the two tandem flexible cylinders in the post-lock-in range deviates from the Strouhal line, which reveals the effect of hydrodynamic interactions on f_{oy} of the two tandem flexible cylinders. It

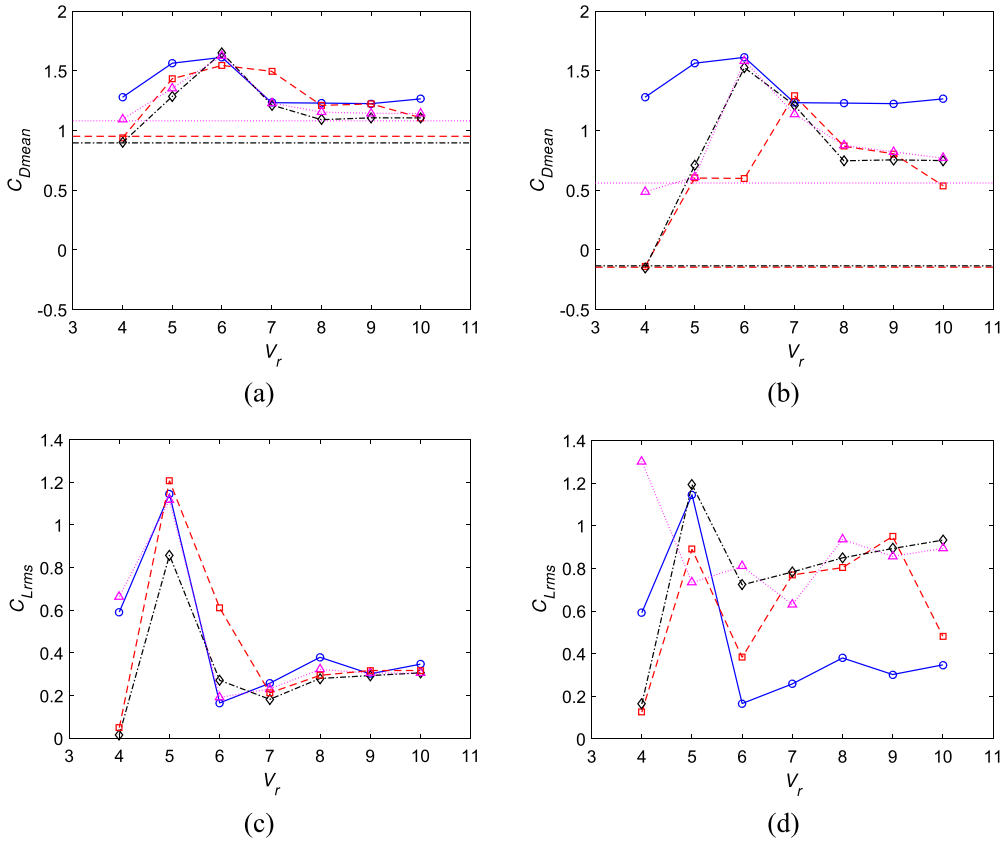

FIG. 14. Variation of total force coefficients with V_r for flexible cylinders: (a) C_{Dmean} of the upstream cylinder, (b) C_{Dmean} of the downstream cylinder, (c) C_{Lrms} of the upstream cylinder, and (d) C_{Lrms} of the downstream cylinder. Blue circles—single flexible cylinder; red squares—tandem S_x/D = 2.5; black diamonds—tandem, S_x/D = 3.5; pink triangles—tandem, S_x/D = 5.

should also be noted that f_{oy} of the downstream cylinder in the post-lock-in range is the same as the corresponding f_{oy} of the upstream cylinder for S_x/D = 2.5 and 3.5. This is related to the aforementioned fact that the vortices rolling up in the gap region between the two cylinders are still connected to the upstream cylinder through the shear layers when they impinge on the downstream cylinder. Consequently, for configurations with S_x/D = 2.5 and 3.5, the oscillation frequencies of the two cylinders in the post-lock-in range are identical.

D. Phase differences between displacements of two tandem flexible cylinders

In this section, the phase differences (ϕ) between the cross-flow displacements at z/L = 0.5 of the two tandem flexible cylinders are analysed. The instantaneous phase difference $\phi(t)$ can be determined by using the concept of the analytical signal,[55] based on Hilbert transforms. In the present study, $\phi(t)$ is calculated for the cases with two cylinders vibrating at an identical frequency in the time range of t = 100–115 s when

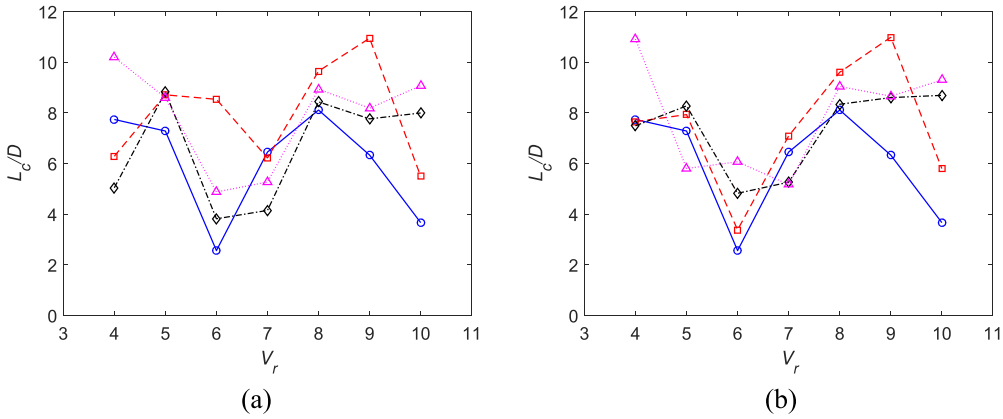

FIG. 15. Variation of correlation lengths with V_r for flexible cylinders: (a) upstream cylinder and (b) downstream cylinder. Blue circles—single flexible cylinder; red squares—tandem S_x/D = 2.5; black diamonds—tandem, S_x/D = 3.5; pink triangles—tandem, S_x/D = 5.

the responses of the two cylinders are in their steady states. In addition, $\phi(t)$ at $V_r = 4$ is excluded as the motions of the cylinders are so small that the computed $\phi(t)$ is not reliable. In all the cases considered, $\phi(t)$ fluctuates around a constant value within the selected time range. Therefore, ϕ is represented by the mean value of $\phi(t)$. Figure 13 illustrates the variations of ϕ with V_r for the three spacing ratios considered in the present study. In Fig. 13, positive ϕ means that y/D of the upstream

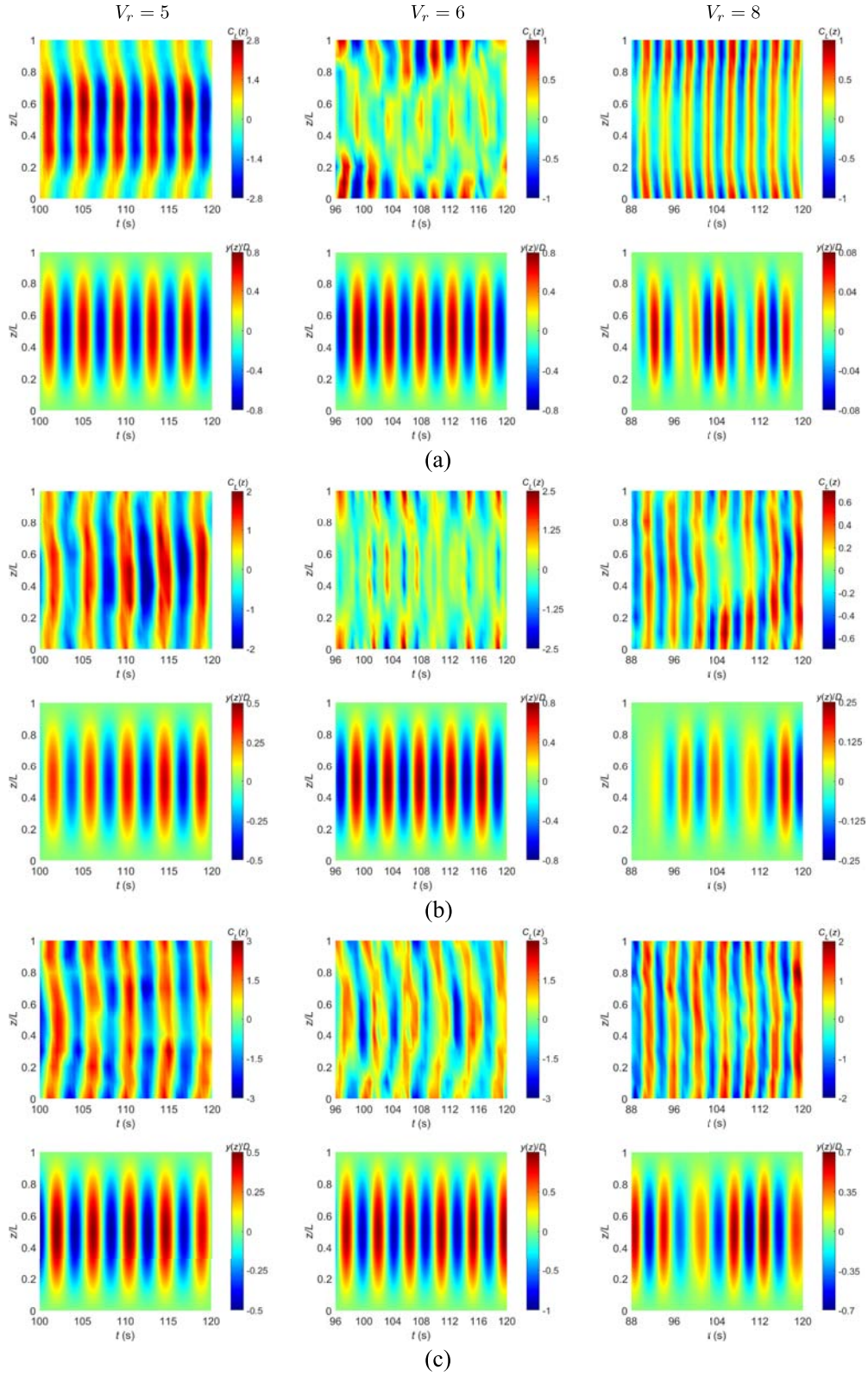

FIG. 16. Contours of sectional lift coefficients and sectional displacements of flexible cylinders: (a) single flexible cylinder, (b) upstream cylinder at $S_x/D = 3.5$, and (c) downstream cylinder at $S_x/D = 3.5$.

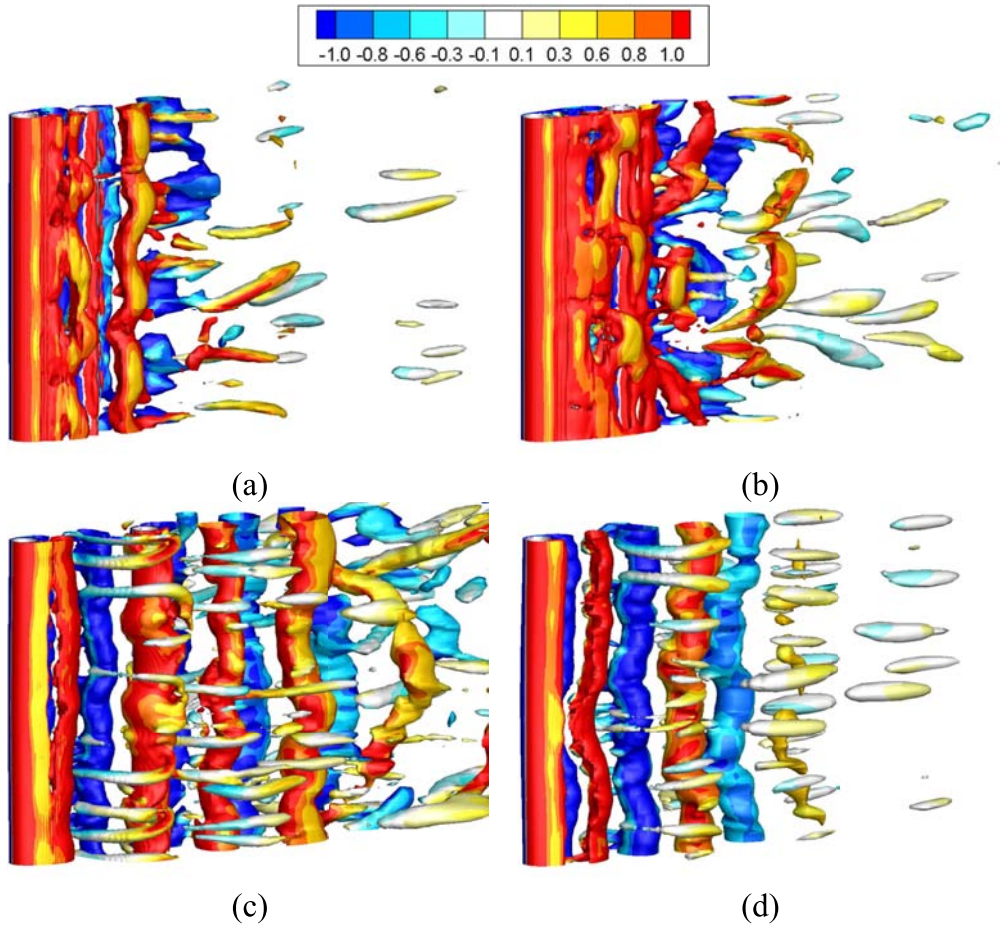

FIG. 17. Iso-surfaces of the eigenvalue $\lambda_2 = -0.1$ with the contours of the spanwise vorticity ω_z on the iso-surfaces for flexible cylinders at $V_r = 4$: (a) $S_x/D = 2.5$, (b) $S_x/D = 3.5$, (c) $S_x/D = 5$ and, (d) single flexible cylinder.

cylinder leads that of the downstream cylinder and negative ϕ indicates that y/D of the upstream cylinder lags that of the downstream cylinder. Based on the changes in the sign of ϕ, it can be concluded that, for each of the three spacing ratios, the phase relation between the displacements of the two tandem flexible cylinders changes twice over the V_r range considered. At $V_r = 5$, ϕ is negative (i.e., y/D of the upstream cylinder lags that of the downstream cylinder) for $S_x/D = 2.5$ and 5 and it becomes positive (i.e., y/D of the upstream cylinder leads that of the downstream cylinder) when V_r increases to 6. With the increase in V_r, the sign of ϕ experiences a second change, taking place in the range of $V_r = 7$–8. As for $S_x/D = 3.5$, the V_r ranges associated with the two changes of the phase relation are the same as those of the other two spacing ratios, whereas the variations in phase relation are opposite. According to the discussion above, the two phase relation changes occur at reduced velocities corresponding to the left of the upper branch and the transition region between the upper and lower branches, respectively. Therefore, it can be speculated that the transitions from one mode of response to another (i.e., from the initial branch to the upper branch and from the upper branch to the lower branch) might have some bearing on the variations of the phase relation between the cross-flow displacements of the two flexible cylinders. Nevertheless, qualitative and quantitative differences in the variations of ϕ with V_r are observed for different spacing ratios reflecting that the phase difference between the cross-flow displacements of the two tandem flexible cylinders depends on V_r and S_x/D. This conclusion agrees with that of Laneville and Brika[58] drawn from their wind tunnel test on the VIV of two tandem flexible cylinders.

E. Hydrodynamic forces

The total drag and lift coefficients are defined as $C_D = F_x/(0.5\rho V^2 DL)$ and $C_L = F_y/(0.5\rho V^2 DL)$, respectively. Here, F_x and F_y represent the total in-line and cross-flow hydrodynamic forces computed by summing the dot product of the pressure and viscous forces with the specified force vector over the cylinder surface. Figures 14(a) and 14(b) show the variation of the mean drag coefficients (C_{Dmean}) with V_r. The constant horizontal lines indicate the values of each cylinder in the stationary system for each S_x/D. At $V_r = 4$, the vibration amplitudes of both cylinders for the three spacing ratios considered are very small. The flow around the two tandem flexible cylinders in Fig. 20 at each S_x/D is essentially similar to that around two tandem stationary cylinders in Fig. 5. Therefore, the mean drag coefficients of both cylinders are close to the values corresponding to the stationary system. Similar to the single flexible cylinder case, the mean drag coefficients of both cylinders reach their maximum values at reduced velocities where the maximum vibration amplitudes appear.

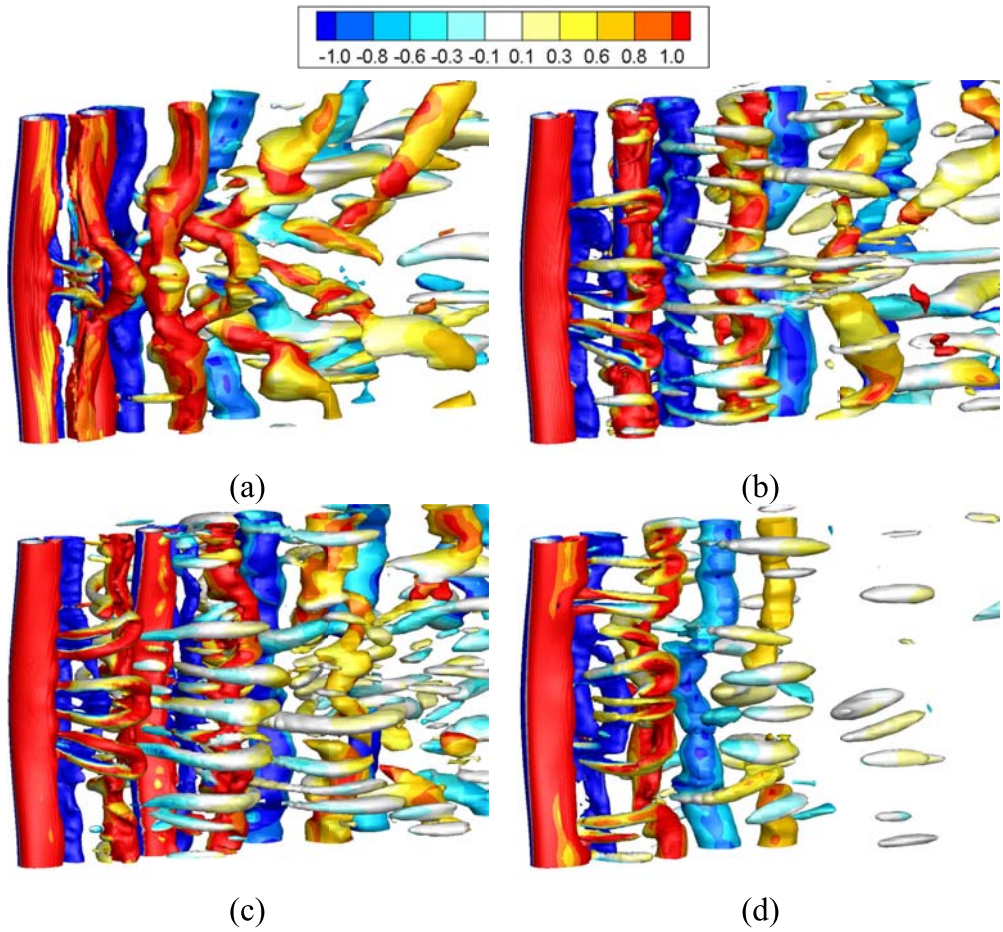

FIG. 18. Iso-surfaces of the eigenvalue $\lambda_2 = -0.1$ with the contours of the spanwise vorticity ω_z on the iso-surfaces for flexible cylinders at $V_r = 6$: (a) $S_x/D = 2.5$, (b) $S_x/D = 3.5$, (c) $S_x/D = 5$, and (d) single flexible cylinder.

For V_r in the post-lock-in range, the values of C_{Dmean} of the upstream cylinder at the three spacing ratios nearly coincide with each other. Overlaps in the C_{Dmean} response curves of the downstream cylinder are observed for $S_x/D = 3.5$ and 5 when $V_r \geq 5$.

Figures 14(c) and 14(d) present the variation of the rms values of the oscillating lift coefficients (C_{Lrms}) with V_r. It shows that the C_{Lrms} response curve of the upstream cylinder at $S_x/D = 5$ resembles that of a single flexible cylinder indicating the negligible effect of the downstream cylinder on the upstream cylinder when $S_x/D = 5$. The maximum C_{Lrms} values of the upstream cylinder for the three spacing ratios considered appear at an identical reduced velocity $V_r = 5$. The C_{Lrms} of the upstream cylinder attains a common value when V_r is large enough that the response of the upstream cylinder is very small for $S_x/D = 3.5$ and 5. This is observed because the oscillations corresponding to those reduced velocities are still large enough to allow vortices to form in the gap region. Similar C_{Lrms} values of the two cylinders are observed at $V_r = 4$ for $S_x/D = 2.5$ and 3.5. The flow patterns in these two cases are essentially similar, namely, the shear layers from the upstream cylinder reattach onto the surface of the downstream cylinder forming a single Kármán vortex street behind the downstream cylinder [Figs. 20(a) and 20(b)]. However, large discrepancies take place in the C_{Lrms} response of the upstream cylinder between $S_x/D = 2.5$ and the other two spacing ratios for $V_r = 6$–9, which reflects that for $S_x/D = 2.5$ the oscillations at those reduced velocities are not large enough for the vortex shedding flow in the gap region to get fully developed. As shown in Fig. 14(d), the C_{Lrms} responses of the downstream cylinder for all the three spacing ratios are quite different from each other and from that of the single flexible cylinder, which highlights that the wake behind the downstream cylinder is a combination of the interacting wakes of the two cylinders.

F. Correlation lengths

The three-dimensionality of the flow in the near wake of the cylinder that determines the fluctuations of the forces acting on the cylinder is measured by the spanwise correlation length. Previous experimental and numerical studies on the VIV of an elastically mounted circular cylinder indicated that there was a sharp drop in the spanwise correlation at the end of the upper branch near the transition between the upper and the lower branches, which does not diminish the response of the cylinder.[37,39,59–62] In the present study, the autocorrelation function as defined in Lucor *et al.*[62] is used to quantify the correlation. The autocorrelation function is described as follows:

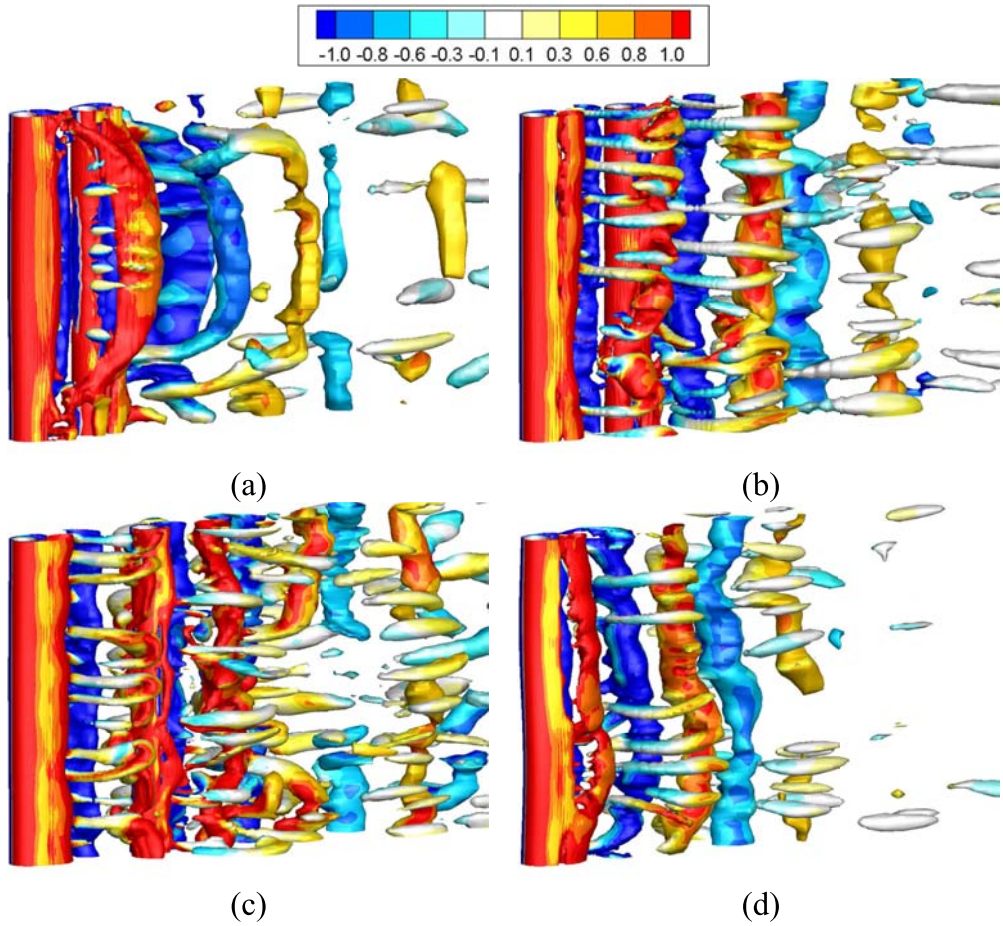

FIG. 19. Iso-surfaces of the eigenvalue $\lambda_2 = -0.1$ with the contours of the spanwise vorticity ω_z on the iso-surfaces for flexible cylinders at $V_r = 10$: (a) $S_x/D = 2.5$, (b) $S_x/D = 3.5$, (c) $S_x/D = 5$, and (d) single flexible cylinder.

$$R(l,t) = \frac{1}{N_t}\sum_{j=1}^{N_t}\left[\frac{(1/N_z)\sum_{i=1}^{N_z} C_L\left(z_i,t_j\right) C_L\left(z_i - l_k, t_j\right)}{(1-N_z)\sum_{i=1}^{N_z} C_L^2\left(z_i,t_j\right)}\right], \tag{10}$$

where $C_L(z_i, t_j)$ is taken to be the fluctuation of the original signal $C_L^*(z_i, t_j)$ from which its mean quantity is subtracted. The signal $C_L(z_i, t_j)$ is given by

$$C_L\left(z_i,t_j\right) = C_L^*\left(z_i,t_j\right) - \frac{1}{N_t}\sum_{n=1}^{N_t} C_L\left(z_i,t_n\right). \tag{11}$$

The shift l_k in Eq. (10) is prescribed to be

$$l_k = k \times l = k \times dz \text{ with } dz = l/N_z \text{ and } k = \left[0, 1, 2, \ldots, \frac{N_z}{2}\right]. \tag{12}$$

The correlation length L_C is then computed by

$$L_C(t) = 2\int_0^{\frac{L/D}{2}} R(l,t)\, dl. \tag{13}$$

Figure 15 shows the variation of the nondimensional correlation lengths (L_C/D) with V_r for flexible cylinders. In general, L_C/D is quite large for low V_r around 4 or 5, representing the initial branch or the left of the upper branch. The large L_C/D is indicative of the strong two-dimensionality of the flow at low V_r. As V_r increases, there is a drop in L_C/D and it reaches its minimum value between $V_r = 6$ and 7, close to the transition region between the upper and lower branches. Finally, L_C/D increases for higher V_r which corresponds to the lower branch of response. Lucor *et al.*[62] conducted a 3D numerical study on the 1DOF VIV of an elastically mounted circular cylinder and observed similar variation trends of L_C/D with V_r. For two tandem stationary cylinders, Wu *et al.*[63] observed that when the two cylinders were close together ($S_x/D < 3$), the downstream cylinder suppressed the shedding of the upstream vortices resulting in the large correlation lengths of the upstream cylinder. As the turbulence intensity and three-dimensionality of the impinging flow on the downstream cylinder were weak, high spanwise correlation was also observed for the downstream cylinder. For most cases with two flexible cylinders in tandem arrangement subject to VIV, the correlation lengths of the two flexible cylinders at $S_x/D = 2.5$ are larger than those for $S_x/D = 3.5$ and 5, which agrees with the conclusion of Wu *et al.*[63] drawn from two tandem stationary cylinders. With the increase of S_x/D, the suppression effect of the downstream cylinder on the upstream vortex shedding diminishes gradually, which leads to similar variations of the upstream cylinder correlation lengths for $S_x/D = 3.5$ and 5 when $V_r \geq 5$. However, as the level and form of the velocity perturbation introduced by the presence of the upstream cylinder depend on the distance between the two cylinders,[63] discrepancies in the correlation

lengths of the downstream cylinder are observed for $S_x/D = 3.5$ and 5.

The variations of the lift coefficients and the displacements along the span at V_r = 5, 6, and 8 are examined by plotting the contours of the sectional lift coefficients [$C_L(z) = F_y(z)/(0.5\rho V^2 D)$, in which the sectional force in the cross-flow direction $F_y(z)$ is obtained by summing up the dot product of the pressure and viscous forces with the specified force vector over a circular cross section] and the sectional displacements [$y(z)/D$] on the z–t plane. The choice of the three reduced velocities stems from the following considerations. $V_r = 5$ represents the large correlation lengths on the left of the upper branch. $V_r = 6$ is near the region where the correlation lengths approach their minimum values and $V_r = 8$ stands for the large correlation lengths in the lower branch. The results for a single flexible cylinder and two tandem flexible cylinders when $S_x/D = 3.5$ are given in Fig. 16. It can be seen that, for the single flexible cylinder and the two tandem flexible cylinders, when L_C/D is large, the distributions of $C_L(z)$ and $y(z)/D$ are well organised. The phase differences between $C_L(z)$ and $y(z)/D$ along the cylinder in each high correlation case are very regular. In contrast, when the correlation is low, $C_L(z)$ signals at different spanwise locations suffer from relative phase shifts despite the fact that $y(z)/D$ signals along the cylinder are nearly in phase. This is caused by the variation of the phase differences between $C_L(z)$ and $y(z)/D$ along the cylinder. The poor phasing between $C_L(z)$ and $y(z)/D$ leads to the decrease of the spanwise correlation.[62]

G. Vortex shedding

One of the objectives of the present study is to investigate the vortex shedding of two tandem flexible cylinders undergoing VIV. The λ_2 method by Jeong and Hussain[64] is used to describe the 3D vortex structures in which λ_2 is the second eigenvalue of the symmetric tensor $\mathbf{S}^2 + \mathbf{\Omega}^2$. Here $\mathbf{S}$ and $\mathbf{\Omega}$ are the symmetric and antisymmetric parts of the velocity gradient tensor $\nabla\mathbf{u}$. Figures 17–19 present the iso-surfaces of $\lambda_2 = -0.1$ at $V_r = 4$, 6, and 10. The iso-surfaces are coloured by ω_z. It can be observed that the wake flow is entirely 3D. The variation of the flow in the spanwise direction is stronger in the cases with smaller correlation lengths. Our previous discussions reveal that the hydrodynamic coefficients of the two tandem flexible cylinders at $V_r = 4$ are close to those of two tandem stationary cylinders. Therefore, it is expected that the 3D vortex structures of the two tandem flexible cylinders at this V_r should be similar to those of two tandem stationary cylinders. It can be seen from Fig. 17 that the 3D vortex

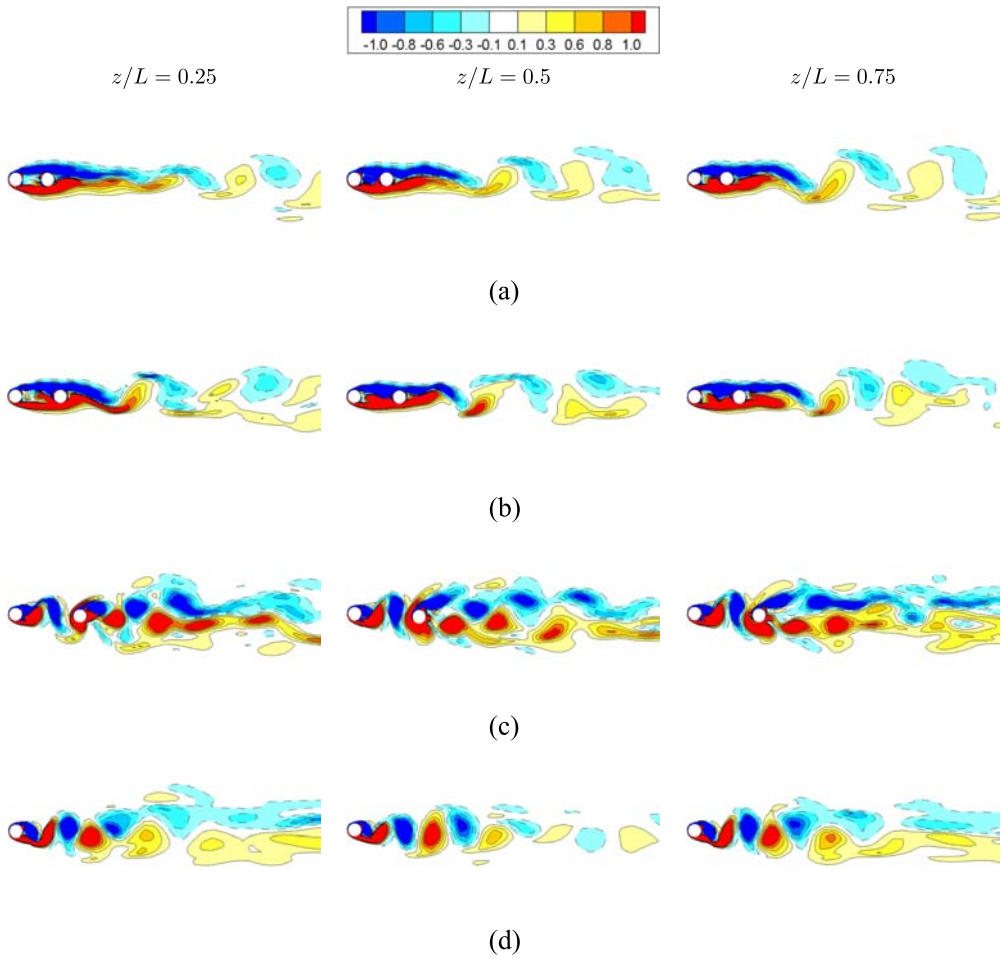

FIG. 20. Contours of spanwise vorticity ω_z on three different cross sections along the flexible cylinders at $V_r = 4$: (a) $S_x/D = 2.5$, (b) $S_x/D = 3.5$, (c) $S_x/D = 5$, and (d) single flexible cylinder.

structures of the flexible cylinders at V_r = 4 do share similar features to that of the corresponding stationary system for each S_x/D in Fig. 4. As shown in Fig. 17, when S_x/D = 2.5 and 3.5, the shear layers from the upstream cylinder reattach onto the surface of the downstream cylinder. When S_x/D increases to 5, vortex shedding occurs in the gap region between the two cylinders and the wake behind the downstream cylinder is a combination of the wakes of the two cylinders. Figure 18 presents the 3D vortex structures of the flexible cylinders at V_r = 6. Compared with the results in Fig. 17, the variation of the flow in the spanwise direction becomes stronger in most of the cases apart from the upstream cylinder at S_x/D = 2.5. In the cases of S_x/D = 2.5 and 3.5 as shown in Figs. 18(a) and 18(b), the oscillations of the two tandem flexible cylinders provide extra time and space for the separated shear layers from the upstream cylinder to roll up into vortices. When V_r increases to 10, the correlation of the spanwise vortices of the flexible cylinders in most of the cases becomes higher than that at V_r = 6 except for the upstream cylinder at S_x/D = 2.5. It is worth noting that although the vibration amplitudes of the two tandem flexible cylinders for S_x/D = 2.5 and 3.5 are quite small at V_r = 10, the shear layers from the upstream cylinder still roll up.

The contours of ω_z on three different cross sections (z/L = 0.25, 0.5, and 0.75) are plotted in order to examine the variation of the flow in the spanwise direction of the flexible cylinders. The three cross sections are chosen in favour of those closer to the cylinder ends to avoid the potential end effect of the periodic boundary condition employed on the two spanwise boundaries. Figure 20 shows ω_z contours of the flexible cylinders on the three cross sections when V_r = 4. The vortex shedding patterns are qualitatively similar to those in Fig. 5 for stationary cylinders. When S_x/D = 2.5 and 3.5, the shear layers from the upstream cylinder reattach onto the surface of the downstream cylinder. At S_x/D = 5, vortex shedding occurs in the gap region between the two cylinders and a binary vortex street forms behind the downstream cylinder. The vortex shedding demonstrates a clear 2S pattern with two single vortices being formed in one cycle as described by Williamson and Roshko.[65] As V_r increases to 6 (Fig. 21), the wake flow behind the flexible cylinders becomes wider. Vortices are formed behind the upstream cylinder in the gap region and these upstream vortices interact with the shear layers of the downstream cylinder when they impinge on the surface of the downstream cylinder. Variation of the vortex shedding modes along the cylinders is observed. The vortex shedding exhibits

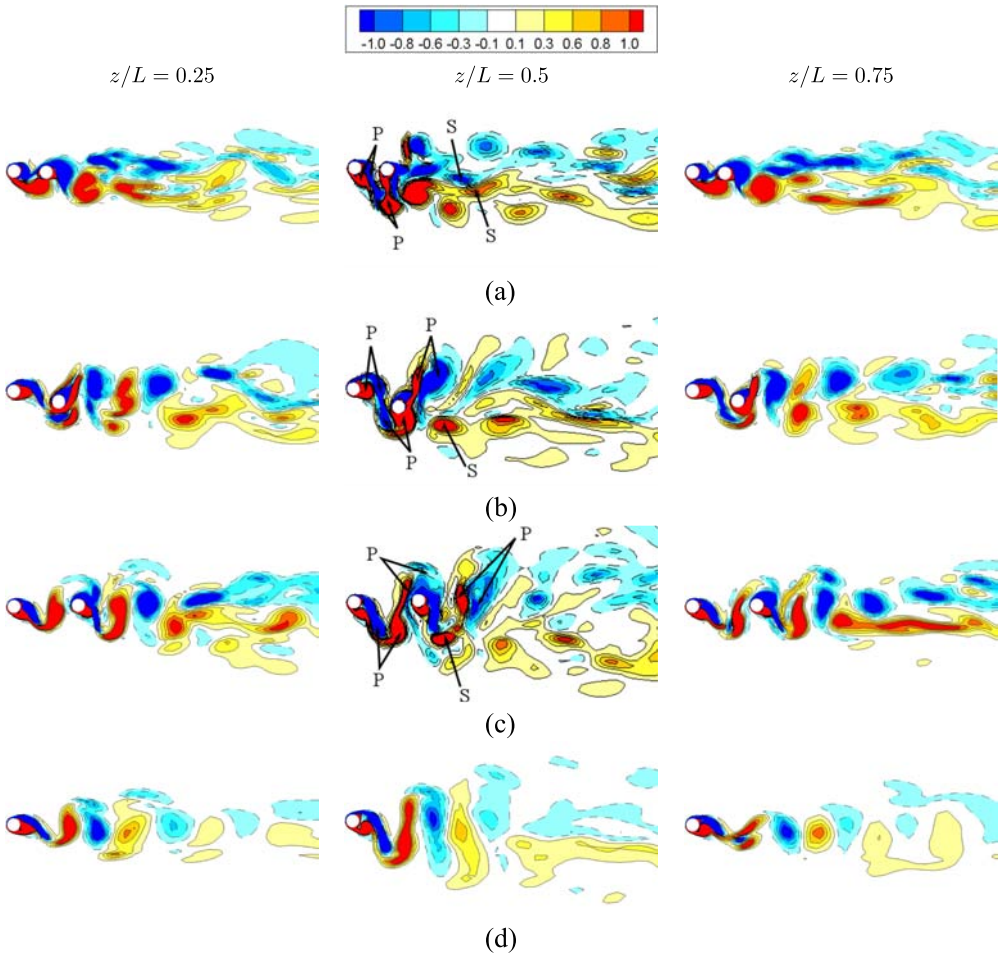

FIG. 21. Contours of spanwise vorticity ω_z on three different cross sections along the flexible cylinders at V_r = 6: (a) S_x/D = 2.5, (b) S_x/D = 3.5, (c) S_x/D = 5, and (d) single flexible cylinder.

a 2S mode at $z/L = 0.25$ and 0.75 where the vibration amplitudes are small. With the increase in the vibration amplitudes towards the middle sections of the cylinders ($z/L = 0.5$), a 2P vortex shedding mode with two pairs of vortices being formed per cycle is observed behind the upstream cylinder. Brika and Laneville[66,67] were the first to show the evidence of the 2P vortex shedding mode in free vibration. The 2P mode at $V_r = 6$ in the present study is qualitatively similar to the 2P mode in the upper branch found by Govardhan and Williamson[57] and Jauvtis and Williamson,[68] in which one vortex of each vortex pair is weaker than the other. This upper-branch 2P mode is associated with the large-amplitude vibration of the upstream cylinder. For the downstream cylinder, a 2S mode is observed at $S_x/D = 2.5$, whereas the vortex shedding for $S_x/D = 3.5$ and 5 shows a P + S mode where the cylinder sheds a single vortex and a vortex pair per cycle. Figure 22 shows the vortex shedding on the middle sections of the two tandem flexible cylinders at different time instants in one vibration cycle when $V_r = 6$ for $S_x/D = 3.5$ and 5. It can be seen that a single vortex and a vortex pair are shed from the downstream cylinder when it moves to its positive and negative peaks, respectively, which confirms the P + S vortex shedding. Although the P + S mode is usually observed in forced vibration experiments,[69,70] it has also been identified in free vibration studies at reduced velocities around the maximum vibration amplitude for an elastically mounted cylinder at low Re[27,39,71] as well as a flexible cylinder undergoing low mode number vibrations.[72] Therefore, the large-amplitude vibration of the downstream cylinder when $S_x/D = 3.5$ and 5 is related to the P + S vortex shedding mode. The variation of the vortex shedding patterns along the cylinders causes the relative phase shifts of $C_L(z)$, which subsequently leads to the decrease of the spanwise correlation. The ω_z contours on three different cross sections along the flexible cylinders at $V_r = 10$ are displayed in Fig. 23. The shear layers from the upstream cylinder are observed to roll up for $S_x/D = 2.5$ and 3.5 despite the fact the vibration amplitudes of the two tandem flexible cylinders are quite small at $V_r = 10$. This confirms the observation from the 3D vortex structures as shown in Fig. 19. When $S_x/D = 2.5$, the vortex shedding patterns of the downstream cylinder vary from a 2S mode at $z/L = 0.25$ and 0.75 to a lower-branch 2P mode at $z/L = 0.5$. Unlike the upper-branch 2P mode observed at $V_r = 6$, the two vortices in each vortex pair of the lower-branch 2P mode at $V_r = 10$ have almost equal strength; thus, the small-amplitude vibration of the downstream cylinder at $S_x/D = 2.5$ is related to the lower-branch 2P mode. A 2S vortex shedding mode is observed for the rest of the cases in Fig. 23.

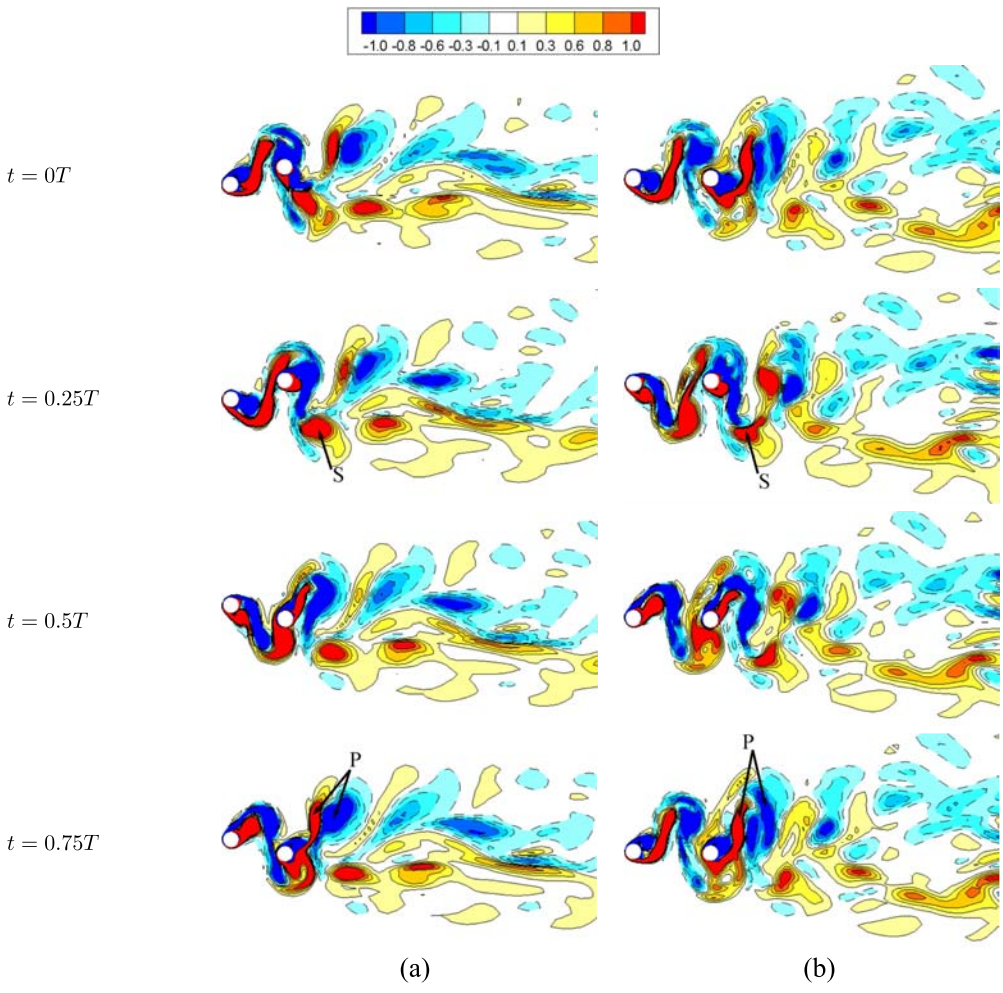

FIG. 22. Contours of spanwise vorticity ω_z on the middle sections of the two tandem flexible cylinders at different time instants in one vibration cycle when $V_r = 6$: (a) $S_x/D = 3.5$ and (b) $S_x/D = 5$.

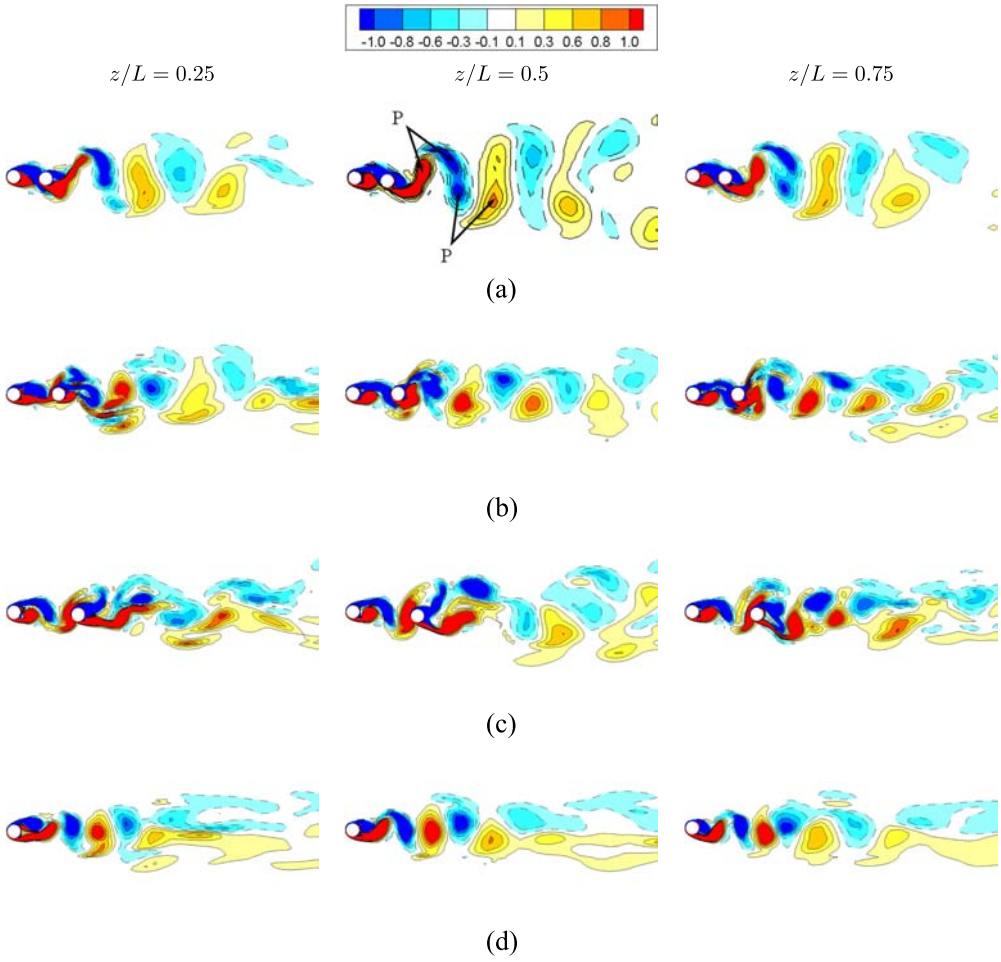

FIG. 23. Contours of spanwise vorticity ω_z on three different cross sections along the flexible cylinders at V_r = 10: (a) S_x/D = 2.5, (b) S_x/D = 3.5, (c) S_x/D = 5, and (d) single flexible cylinder.

V. CONCLUSIONS

The effect of spacing on the cross-flow vortex-induced vibrations of two tandem flexible cylinders is numerically studied at Re = 500 using a two-way fluid-structure interaction method. A moderate mass ratio m^* = 10, a length-to-diameter ratio L/D = 12, and zero structural damping are considered in the simulation. The reduced velocity ranges from 4 to 10 in which the flexible cylinders mainly vibrate in the first mode. Three spacing ratios (S_x/D = 2.5, 3.5, and 5) are examined. Based on the numerical results, the effect of spacing on the hydrodynamic interactions and the VIV responses of the two tandem flexible cylinders is investigated. In particular, the aspects that are rarely reported in previous studies such as the correlation lengths and the three-dimensional flow structures of two tandem flexible cylinders are provided. The conclusions are summarised as follows.

The upstream cylinder shows a classical VIV response for the three spacing ratios considered. As the vortices impinging on the downstream cylinder are still connected to the shear layers of the upstream cylinder in the cases of small spacing ratios, the response of the downstream cylinder is also similar to a typical VIV response. When the spacing between the two tandem flexible cylinders is large enough for the vortices to be shed from the upstream cylinder, the downstream cylinder undergoes WIV with large amplitudes at high reduced velocities and an extended lock-in range. However, in contrast to an elastically mounted downstream cylinder whose response can be divided into three regimes, only the first two regimes appear in the present study. The third response regime is not observed due to the fact that the flexible downstream cylinder with two fixed ends has an infinite number of natural frequencies and the natural frequencies of two neighbouring vibration modes are very close. As a constant Re is used in the present study, a flattened amplitude response is observed in the second response regime of the downstream cylinder.

It is found that there exist two changes of the phase relation between the cross-flow displacements of the two flexible cylinders arranged in tandem. The reduced velocity ranges associated with the phase relation changes correspond to the left of the upper branch and the transition between the upper and lower branches, respectively. Thus, the variations of phase relation between the cross-flow displacements of the two tandem flexible cylinders are presumed to be related to the transitions from the initial branch to the upper branch and from the upper branch to the lower branch. The phase differences between the cross-flow displacements of the two tandem flexible cylinders

are also found to differ for different reduced velocities and spacing ratios.

At very low reduced velocities when the vibration amplitudes of the two tandem flexible cylinders are small, the flow around the two tandem flexible cylinders is essentially similar to that around two tandem stationary cylinders. Consequently, the hydrodynamic force coefficients are close to the values corresponding to the stationary system. The effect of the downstream cylinder on the upstream cylinder is nearly negligible for large spacing ratios and for small spacing ratios, the oscillations in the classical VIV resonance range are not large enough for the vortex shedding to fully develop in the gap region. For two vibrating flexible cylinders in tandem arrangement, the wake behind the downstream cylinder consists of the interacting wakes of the two cylinders.

The variation of the correlation lengths of the two tandem flexible cylinders with the reduced velocity roughly follows that of an elastically mounted circular cylinder. In particular, the correlation lengths experience a sharp drop at reduced velocities around the mode transition between the upper and lower branches. For small spacing ratios, the presence of the downstream cylinder suppresses the three-dimensionality of the upstream flow resulting in the large correlation lengths of the upstream cylinder, and the subsequent weak turbulence intensity and three-dimensionality of the upstream flow consequently lead to high spanwise correlation of the downstream cylinder. Large correlation lengths are found to be associated with regular phase differences between the sectional lift forces and sectional displacements along the cylinder, whereas the decrease of the spanwise correlation is attributed to the poor phasing between the forces and the displacements.

The flow around two flexible cylinders in tandem arrangement that are subject to VIV is totally three-dimensional. The flow in the spanwise direction suffers stronger variations when the correlation is poor. In the case with spacing ratios corresponding to the reattachment regime of two tandem stationary cylinders, the large-amplitude vibrations of the two tandem flexible cylinders in the resonance range provide the time and space for the vortices to roll up in the gap. The wake in the lock-in range is found to be wider than that in the non-lock-in range. 2S, 2P, and P + S vortex shedding modes are identified in the present study. The upper-branch 2P mode with one vortex being stronger than the other in each vortex pair is found to be associated with the large-amplitude vibration of the upstream cylinder in the lock-in range and the P + S mode is related to the large-amplitude vibration of the downstream cylinder for S_x/D = 3.5 and 5. In contrast, the lower-branch 2P mode with two equal-strength vortices in each vortex pair leads to the lower-branch response of the downstream cylinder at high reduced velocity at S_x/D = 2.5. Variation of the vortex shedding modes in the spanwise direction is observed in the cases with low spanwise correlation.

Overall, the present results confirmed various important conclusions obtained from previous experimental studies. Additionally, they also highlighted some new aspects such as the disappearance of the third response regime for a flexible downstream cylinder with two fixed ends at large spacing ratios and also the transitions between different response branches (i.e., between the initial branch and the upper branch and between the upper branch and the lower branch) may explain the changes in the phase relation between the cross-flow displacements of the two flexible cylinders in tandem arrangement. Furthermore, the correlation lengths and the 3D flow structures that are difficult to obtain in the experimental studies are provided. As the present study is one of the first few numerical investigations on the VIV of two tandem flexible cylinders, there are also some limitations. The Reynolds number used in the numerical simulation is fixed with the consequence that the monotonically increasing amplitude in the second response regime of the flexible downstream cylinder at large spacing ratios was not observed. A further limitation in this regard is that the present study is focused on a low Reynolds number regime. The maximum vibration amplitudes will be larger if a higher Reynolds number range is considered. The Reynolds number also influences the critical spacing of the two tandem flexible cylinders. The responses of the two tandem flexible cylinders, especially when S_x/D = 3.5, might change if the Reynolds number is different. Moreover, the vibrations of the two tandem flexible cylinders in the present study are confined in the cross-flow direction. As we considered a moderate mass ratio, the effect of the in-line degree of freedom on the maximum vibration amplitudes may not be very pronounced. However, the in-line motion may have an impact on other aspects of the VIV responses of the two tandem flexible cylinders as it will change the gap between the two cylinders when they vibrate. Given the limitations of the present study, future research on coupled in-line and cross-flow VIV of two tandem flexible cylinders in a higher Re range is worthwhile.

ACKNOWLEDGMENTS

Results were obtained using the EPSRC funded ARCHIE-WeSt High Performance Computer (www.archie-west.ac.uk). EPSRC Grant No. EP/K000586/1.

[1] R. D. Blevins, *Flow-Induced Vibration* (Van Nostrand Reinhold Company, New York, USA, 1977).
[2] T. Sarpkaya, "Vortex-induced oscillations: A selective review," J. Appl. Mech. **46**, 241–258 (1979).
[3] P. W. Bearman, "Vortex shedding from oscillating bluff bodies," Annu. Rev. Fluid Mech. **16**, 195–222 (1984).
[4] C. H. K. Williamson and R. Govardhan, "Vortex-induced vibrations," Annu. Rev. Fluid Mech. **36**, 413–455 (2004).
[5] R. D. Gabbai and H. Benaroya, "An overview of modelling and experiments of vortex-induced vibrations of circular cylinders," J. Sound Vib. **282**, 575–646 (2005).
[6] B. M. Sumer and J. Fredsøe, *Hydrodynamics Around Cylindrical Structures* (World Scientific Publishing Co. Pte. Ltd., London, UK, 2006).
[7] P. W. Bearman, "Circular cylinder wakes and vortex-induced vibrations," J. Fluids Struct. **27**, 648–658 (2011).
[8] X. Wu, F. Ge, and Y. Hong, "A review of recent studies on vortex-induced vibrations of long slender cylinders," J. Fluids Struct. **28**, 292–308 (2012).
[9] M. P. Païdoussis, S. J. Price, and E. de Langre, *Fluid-Structure Interactions: Cross-Flow-Induced Instabilities* (Cambridge University Press, New York, USA, 2014).
[10] M. S. Triantafyllou, R. Bourguet, J. M. Dahl, and Y. Modarres-Sadeghi, *Vortex-Induced Vibrations* (Springer International Publishing, London, UK, 2016).
[11] M. M. Zdravkovich, "The effects of interference between circular cylinders in cross flow," J. Fluids Struct. **1**, 239–261 (1987).

[12]T. Igarashi, "Characteristics of the flow around two circular cylinders arranged in tandem: 1st report," Bull. JSME **24**, 323–331 (1981).
[13]F. S. Hover and M. S. Triantafyllou, "Galloping response of a cylinder with upstream wake interference," J. Fluids Struct. **15**, 503–512 (2001).
[14]G. R. S. Assi, P. W. Bearman, and J. R. Meneghini, "On the wake-induced vibration of tandem circular cylinders: The vortex interaction excitation mechanism," J. Fluid Mech. **661**, 365–401 (2010).
[15]G. R. S. Assi, P. W. Bearman, B. S. Carmo, J. R. Meneghini, S. J. Sherwin, and R. H. J. Willden, "The role of wake stiffness on the wake-induced vibration of the downstream cylinder of a tandem pair," J. Fluid Mech. **718**, 201–245 (2013).
[16]M. M. Zdravkovich, "Flow induced oscillations of two interfering circular cylinders," J. Sound Vib. **101**, 511–521 (1985).
[17]D. Brika and A. Laneville, "Wake interference between two circular cylinders," J. Wind Eng. Ind. Aerodyn. **72**, 61–70 (1997).
[18]D. Brika and A. Laneville, "The flow interaction between a stationary cylinder and a downstream flexible cylinder," J. Fluids Struct. **13**, 579–606 (1999).
[19]F. J. Huera-Huarte and P. W. Bearman, "Vortex and wake-induced vibrations of a tandem arrangement of two flexible circular cylinders with near wake interference," J. Fluids Struct. **27**, 193–211 (2011).
[20]F. J. Huera-Huarte and M. Gharib, "Vortex- and wake-induced vibrations of a tandem arrangement of two flexible circular cylinders with far wake interference," J. Fluids Struct. **27**, 824–828 (2011).
[21]B. S. Carmo, S. J. Sherwin, P. W. Bearman, and R. H. J. Willden, "Flow-induced vibration of a circular cylinder subjected to wake interference at low Reynolds number," J. Fluids Struct. **27**, 503–522 (2011).
[22]B. S. Carmo, G. R. S. Assi, and J. R. Meneghini, "Computational simulation of flow-induced vibration of a circular cylinder subjected to wake interference," J. Fluids Struct. **41**, 99–108 (2013).
[23]M. Zhao, "Flow induced vibration of two rigidly coupled circular cylinders in tandem and side-by-side arrangements at a low Reynolds number of 150," Phys. Fluids **25**, 123601-1–123601-31 (2013).
[24]L. Ding, L. Zhang, C. Wu, E. S. Kim, and M. M. Bernitsas, "Numerical study on the effect of tandem spacing on flow-induced motions of two cylinders with passive turbulence control," J. Offshore Mech. Arct. Eng. **139**, 021801-1–021801-8 (2017).
[25]G. V. Papaioannou, D. K. P. Yue, M. S. Triantafyllou, and G. E. Karniadakis, "On the effect of spacing on the vortex-induced vibrations of two tandem cylinders," J. Fluids Struct. **24**, 833–854 (2008).
[26]T. K. Prasanth and S. Mittal, "Flow-induced oscillation of two circular cylinders in tandem arrangement at low Re," J. Fluids Struct. **25**, 1029–1048 (2009).
[27]Y. Bao, C. Huang, D. Zhou, J. Tu, and Z. Han, "Two-degree-of-freedom flow-induced vibrations on isolated and tandem cylinders with varying natural frequency ratios," J. Fluids Struct. **35**, 50–75 (2012).
[28]H. C. Chen, C. R. Chen, and K. Huang, "CFD simulation of vortex-induced and wake-induced vibrations of dual vertical risers," presented at the 23rd International Offshore and Polar Engineering Conference, Anchorage, USA, 2013.
[29]L. M. González, A. Rodriguez, C. A. Garrido, J. C. Suarez, and F. J. Huera Huarte, "CFD simualtion on the vortex-induced vibrations of a flexible cylinder with wake interference," OMAE2015–41128, St. Johns, Canada, 2015.
[30]F. J. Huera-Huarte, Z. A. Bangash, and L. M. González, "Towing tank experiments on the vortex-induced vibrations of a flexible cylinder with wake interference," OMAE2014–23873, San Francisco, California, USA, 2014.
[31]ANSYS Inc., ANSYS Mechanical APDL Coupled-field Analysis Guide, Canonsburg, USA, 2013.
[32]ANSYS Inc., ANSYS CFX-solver Theory Guide, Canonsburg, USA, 2013.
[33]C. Rhie and W. Chow, "A numerical study of the turbulent flow past an isolated airfoil with trailing edge separation," in *3rd Joint Thermophysics, Fluids, Plasma and Heat Transfer Conference* (AIAA, St. Louis, USA, 1982).
[34]T. J. Barth and D. C. Jespersen, "The design and application of upwind schemes on unstructured meshes," in *27th Aerospace Sciences Meeting* (AIAA, Reno, USA, 1989).
[35]H. M. Hilber, T. J. R. Hughes, and R. L. Taylor, "Improved numerical dissipation for time integration algorithms in structural dynamics," Earthquake Eng. Struct. Dyn. **5**, 283–292 (1977).
[36]ANSYS Inc., ANSYS Mechanical APDL Element Reference, Canonsburg, USA, 2013.
[37]M. Zhao, L. Cheng, H. An, and L. Lu, "Three-dimensional numerical simulation of vortex-induced vibration of an elastically mounted rigid circular cylinder in steady current," J. Fluids Struct. **50**, 292–311 (2014).
[38]E. Wang and Q. Xiao, "Numerical simulation of vortex-induced vibration of a vertical riser in uniform and linearly sheared currents," Ocean Eng. **121**, 492–515 (2016).
[39]E. Wang, Q. Xiao, and A. Incecik, "Three-dimensional numerical simulation of two-degree-of-freedom VIV of a circular cylinder with varying natural frequency ratios at Re = 500," J. Fluids Struct. **73**, 162–182 (2017).
[40]C. Evangelinos and G. E. Karniadakis, "Dynamics and flow structures in the turbulent of rigid and flexible cylinders subject to vortex-induced vibrations," J. Fluid Mech. **400**, 91–124 (1999).
[41]C. Evangelinos, D. Lucor, and G. E. Karniadakis, "DNS-derived force distribution on flexible cylinders subject to vortex-induced vibration," J. Fluids Struct. **14**, 429–440 (2000).
[42]F. Xie, J. Deng, Q. Xiao, and Y. Zheng, "A numerical simulation of VIV on a flexible circular cylinder," Fluid Dyn. Res. **44**, 045508 (2012).
[43]G. V. Papaioannou, D. K. P. Yue, M. S. Triantafyllou, and G. E. Karniadakis, "Three-dimensionality effect in flow around two tandem cylinders," J. Fluid Mech. **558**, 387–413 (2006).
[44]T. Igarashi, "Characteristics of the flow around two circular cylinders arranged in tandem (second report, unique flow phenomenon at small spacing)," Bull. JSME **27**, 2380–2387 (1984).
[45]G. V. Papaioannou, "A numerical study of flow-structure interactions with application to flow past a pair of cylinders," Ph.D. thesis, Massachusetts Institute of Technology, Massachusetts, USA, 2004.
[46]G. Xu and Y. Zhou, "Strouhal numbers in the wake of two inline cylinders," Exp. Fluids **37**, 248–256 (2004).
[47]Y. Zhou and M. W. Yiu, "Flow structure, momentum and heat transport in a two-tandem-cylinder wake," J. Fluid Mech. **548**, 17–48 (2006).
[48]B. S. Carmo, J. R. Meneghini, and S. J. Sherwin, "Possible states in the flow around two circular cylinders in tandem with separations in the vicinity of the drag inversion spacing," Phys. Fluids **22**, 054101 (2010).
[49]B. S. Carmo, J. R. Meneghini, and S. J. Sherwin, "Secondary instabilities in the flow around two circular cylinders in tandem," J. Fluid Mech. **644**, 395–431 (2010).
[50]D. Sumner, "Two circular cylinders in cross-flow: A review," J. Fluids Struct. **26**, 849–899 (2010).
[51]E. Lehn, VIV Suppression Tests on High L/D Flexible Cylinders, Norwegian Marine Technology Research Institute, Trondheim, Norway, 2003.
[52]M. Zhao and L. Cheng, "Vortex-induced vibration of a circular cylinder of finite length," Phys. Fluids **26**, 015111-1–015111-26 (2014).
[53]M. Zhao and L. Cheng, "Numerical simulation of two-degree-of-freedom vortex-induced vibration of a circular cylinder close to a plane boundary," J. Fluids Struct. **27**, 1097–1110 (2011).
[54]F. J. Huera-Huarte and P. W. Bearman, "Wake structures and vortex-induced vibrations of a long flexible cylinder - Part I: Dynamic response," J. Fluids Struct. **25**, 969–990 (2009).
[55]A. Pikovsky, M. Rosenblum, and J. Kurths, *Synchronisation: A Universal Concept in Nonlinear Sciences* (Cambridge University Press, New York, USA, 2001).
[56]L. Ljungkrona and B. Sundén, "Flow visualisation and surface pressure measurement on two tubes in an inline arrangement," Exp. Therm. Fluid Sci. **6**, 15–27 (1993).
[57]R. Govardhan and C. H. K. Williamson, "Modes of vortex formation and frequency response for a freely-vibrating cylinder," J. Fluid Mech. **420**, 85–130 (2000).
[58]A. Laneville and D. Brika, "The fluid and mechanical coupling between two circular cylinders in tandem arrangement," J. Fluids Struct. **13**, 967–986 (1999).
[59]F. S. Hover, A. H. Techet, and M. S. Triantafyllou, "Forces on oscillating uniform and tapered cylinders in crossflow," J. Fluid Mech. **363**, 97–114 (1998).
[60]F. S. Hover, J. T. Davis, and M. S. Triantafyllou, "Three-dimensional mode transition in vortex-induced vibrations of a circular cylinder," Eur. J. Mech.-B/Fluids **23**, 29–40 (2004).
[61]D. Lucor, J. Foo, and G. E. Karniadakis, "Correlation length and force phasing of a rigid cylinder subject to VIV," presented at the IUTAM Symposium on Integrated Modeling of Fully Coupled Fluid Structure Interactions Using Analysis, Computations and Experiments, New Jersey, USA, 2003.

[62]D. Lucor, J. Foo, and G. E. Karniadakis, "Vortex mode selection of a rigid cylinder subject to VIV at low mass-damping," J. Fluids Struct. **20**, 483–503 (2005).
[63]J. Wu, L. W. Welch, M. C. Welsh, J. Sheridan, and G. J. Walker, "Spanwise wake structures of a circular cylinder and two circular cylinders in tandem," Exp. Therm. Fluid Sci. **9**, 299–308 (1994).
[64]J. Jeong and F. Hussain, "On the identification of a vortex," J. Fluid Mech. **285**, 69–94 (1995).
[65]C. H. K. Williamson and A. Roshko, "Vortex formation in the wake of an oscillating cylinder," J. Fluids Struct. **2**, 355–381 (1988).
[66]D. Brika and A. Laneville, "Vortex-induced vibrations of a long flexible circular cylinder," J. Fluid Mech. **250**, 481–508 (1993).
[67]D. Brika and A. Laneville, "An experimental study of the aeolian vibrations of a flexible circular cylinder at different incidences," J. Fluids Struct. **9**, 371–391 (1995).
[68]N. Jauvtis and C. H. K. Williamson, "The effect of two degrees of freedom on vortex-induced vibration at low mass and damping," J. Fluid Mech. **509**, 23–62 (2004).
[69]O. M. Griffin and S. E. Ramberg, "The vortex street wakes of vibrating cylinders," J. Fluid Mech. **66**, 553–576 (1974).
[70]R. Zdero, Ö. F. Turan, and D. G. Havard, "Towards understanding galloping: Near-wake study of oscillating smooth and stranded circular cylinders in forced motion," Exp. Therm. Fluid Sci. **10**, 28–43 (1995).
[71]S. P. Singh and S. Mittal, "Vortex-induced oscillations at low Reynolds numbers: Hysteresis and vortex shedding modes," J. Fluids Struct. **20**, 1085–1104 (2005).
[72]E. D. Gedikli and J. M. Dahl, "Mode shape vibration for a low-mode number flexible cylinder subject to vortex-induced vibrations," in *ASME 2014 33rd International Conference on Ocean, Offshore and Arctic Engineering* (ASME, San Francisco, USA, 2014).